https://doi.org/10.5194/egusphere-2025-244
Preprint. Discussion started: 26 March 2025

Enhanced Baseflow Separation in Rural Catchments: Event-Specific Calibration of Recursive Digital Filters with Tracer-Derived Data

Fernanda Helfer[1], Felipe Bernardi[2], Claudia Alessandra Peixoto de Barros[3], Daniel Gustavo Allasia[2], Jean Paolo Gomes Minella[4], Rutinéia Tassi[2], Néverton Scariot[2]

[1]School of Engineering and Built Environment, Griffith University, Gold Coast, QLD, 4222, Australia
[2]Sanitary and Environmental Engineering Department, Federal University of Santa Maria, Santa Maria, RS, 97105-900, Brazil.
[3]Soil Department, Federal University of Rio Grande do Sul, Porto Alegre, RS, 91540-000, Brazil.
[4]Soil Department, Federal University of Santa Maria. Santa Maria, RS, 97105-900, Brazil.

Correspondence to: Fernanda Helfer (f.helfer@griffith.edu.au)

Abstract: This study investigates the performance of baseflow separation methods in a small rural catchment, emphasizing the calibration of three Recursive Digital Filters (RDFs): Eckhardt, Lyne and Hollick (LH), and Chapman and Maxwell (CM). By integrating dissolved silica concentration as a reference tracer, the study refines the parameterization of BFI_{max} in the Eckhardt's filter and *Beta* in the LH filter. An innovative event-specific calibration methodology was applied, where rainfall events were categorized by intensity to tailor filter parameters accordingly. Results indicate that the Eckhardt's filter, when calibrated dynamically per event magnitude, yields the most accurate baseflow estimates, closely aligning with observed data. The event-based calibration significantly enhanced accuracy, particularly for the Eckhardt's and LH filters, compared to a general calibration method. The CM filter, despite generating reasonable hydrograph shapes, consistently underestimated baseflow due to its fixed parameters. These findings highlight the necessity of customized calibration strategies for improved baseflow separation and underscore the superior performance of the Eckhardt's filter when integrated with event-specific calibrations. This research offers practical insights for hydrologists aiming to optimize baseflow modeling in rural catchments, contributing to improved water resource management and conservation.

https://doi.org/10.5194/egusphere-2025-244
Preprint. Discussion started: 26 March 2025

1. Introduction

Baseflow, a key hydrological component sustaining river flow during dry periods, originates from groundwater discharge and delayed subsurface contributions. Accurate quantification of baseflow is essential for managing water resources, designing infrastructure, and maintaining ecological stability (Apurv & Cai, 2020; Beatty et al., 2010; Glas et al., 2023; Gómez et al., 2020; Miller et al., 2016; Murray et al., 2003; Walker, 2023). However, direct measurement remains challenging due to complex interactions between surface and subsurface hydrological processes.

Measuring baseflow presents significant challenges, often requiring extensive resources due to the reliance on tracer-based methodologies or aquifer-level monitoring, both of which can be costly and time-intensive (Vasconcelos et al., 2013). To address these limitations, Recursive Digital Filters (RDFs) have been developed as an alternative approach for estimating baseflow using streamflow data (Chapman & Maxwell, 1996; Eckhardt, 2005; Furey & Gupta, 2001; Lyne & Hollick, 1979). Although most RDFs do not explicitly simulate the underlying physical mechanisms governing baseflow – except for the model proposed by Furey & Gupta (2001) – they remain widely utilized in hydrological studies. These methods are particularly valued for their ability to produce hydrologically plausible baseflow hydrographs with smooth transitions (Xie et al., 2020), generate consistent and reproducible results (Arnold et al., 1995; Ladson et al., 2013; Su et al., 2016), and offer computational efficiency, making them easy to implement and automate (Li et al., 2013; Su et al., 2016).

In addition to streamflow data, RDFs require specific parameters that are designed to accentuate the slowly changing, persistent characteristics associated with baseflow hydrographs, while attenuating the faster fluctuations related to quickflow (Chapman & Maxwell, 1996; Eckhardt, 2005, 2008; Lyne & Hollick, 1979; Nathan & Mcmahon, 1990; Sloto & Crouse, 1996). Therefore, choosing the right parameters is crucial for RDFs to produce reliable outcomes. There is a growing trend towards utilizing independent baseflow estimates (such as tracer-based baseflow) in RDF calibration (Gonzales et al., 2009; Helfer et al., 2024), even though the filters offer non-calibration opportunity, with the selection or derivation of filter parameters based on catchment characteristics (Chapman & Maxwell, 1996; Eckhardt, 2005; Nathan & Mcmahon, 1990).

The simplest RDF filters are those that rely on one single parameter. Two widely used one-parameter filters are the models developed by Lyne and Hollick (1979), referred to as 'LH', and Chapman and Maxwell (1996), referred to as 'CM'. The LH model is expressed as:

$$qfLH_t = \beta \times qfLH_{t-1} + \frac{1+\beta}{2} \times (q_t - q_{t-1}) \quad , \quad \text{subject to } qf_t \geq 0 \tag{1}$$

where $qfLH_t$ is the quickflow at time t, $qfLH_{t-1}$ is the quickflow at time $t-1$, q_t is the total streamflow at time t, and q_{t-1} is the total streamflow at time $t-1$. The filter parameter, β, regulates the separation process. Baseflow at each timestep, $qbLH_t$, is determined by subtracting quickflow from the total streamflow, following the equation $qbLH_t = q_t - qfLH_t$. This filtering process is typically executed in three iterations: a forward pass, a backward pass (where the $t-1$ timestep is replaced by $t+1$), and a final forward pass. During the first forward pass, q_t is substituted with the baseflow calculated in the preceding pass.

https://doi.org/10.5194/egusphere-2025-244
Preprint. Discussion started: 26 March 2025

These sequential iterations help to refine the baseflow hydrograph by smoothing fluctuations and introducing a slight delay in the baseflow peak relative to quickflow (Murphy et al., 2011).

For the *Beta* parameter (β), the common reference value is 0.925 (Arnold & Allen, 1999; Arnold et al., 1995; Ladson et al., 2013; Nathan & Mcmahon, 1990), with values within the range 0.90 – 0.95 claimed to yield the most reliable baseflow hydrographs (Nathan & Mcmahon, 1990). However, comparisons of modelled and measured baseflow values derived from tracer observations have indicated optimal values above this range. For example, a study in the Murray Darling Basin by CSIRO & SKM (2010) reported by Ladson et al. (2013) found a *Beta* value of 0.98 to yield more accurate baseflow separations. This finding is supported by Zhang et al. (2017), who identified *Beta* values between 0.943 to 0.987 across five Australian catchments as more effective. Li et al. (2013) noted the limitations of the 0.925 *Beta* parameter, especially in catchments with soils of low hydraulic conductivity, pointing out the necessity for catchment-specific calibrations due to the filter's sensitivity. Conversely, Mau and Winter (1997) identified a *Beta* value of 0.85 as optimal for a small mountain catchment in New Hampshire, noting that values above 0.85 led to unrealistic baseflow estimates. The recommendations to utilize the recession constant as the *Beta* parameter by researchers such as Eckhardt (2005), Tan et al. (2009a), Zhang et al. (2017), Mugo and Sharma (1999) accentuate the variability in selecting appropriate *Beta* values across hydrological studies. This variability emphasizes the need for further investigation and catchment-specific adjustments, as reinforced by Ladson et al. (2013). This calibration becomes even more important due to the high sensitivity of the filter to the *Beta* parameter. For instance, Nathan and Mcmahon (1990) observed that a ±3% change in the parameter could alter the baseflow index (*BFI* – the long-term ratio of baseflow volume to the total volume of streamflow) value by as much as +14% and -26%, highlighting the critical nature of precise *Beta* parameter selection.

Despite these challenges in parameter determination, the LH method has been extensively applied in hydrology. It is the approach used in the "*Low flow atlas for Victorian streams*" (Nathan & Weinmann, 1993) and the method recommended by the "*Australian Rainfall and Runoff*" guidelines (Murphy et al., 2011). It is also the algorithm used in the BFLOW program (Arnold & Allen, 1999). Other examples include the work by Lacey and Grayson (1998), who applied the method in 114 catchments with areas < 192 km^2 in Victoria (Australia), the work by Nathan and McMahon (1992), who applied the method to 186 catchments in Victoria and New South Wales (Australia), research by Mugo and Sharma (1999) who applied the filter in three catchments in Kenya with areas ranging from 0.36 to 0.65 km^2, and the studies by Tan et al. (2009a; 2009b), who applied the method to a 5.6 km^2 in Singapore.

The CM model (Chapman & Maxwell, 1996) is another one-parameter filter and is given as:

$$qbCM_t = \frac{a}{2-a} \times qbCM_{t-1} + \frac{1-a}{2-a} \times q_t \quad (2)$$

https://doi.org/10.5194/egusphere-2025-244
Preprint. Discussion started: 26 March 2025

where $qbCM_t$ is the CM filter baseflow at time t, $qbCM_{t-1}$ is the CM filter baseflow at time $t-1$, and a is the filter parameter, given by the baseflow recession constant. In the CM and LH models, when the calculated baseflow at a specific time step exceeds the total streamflow, the baseflow value is capped at the total streamflow value.

The CM method has been largely studied and applied in hydrology (Chapman & Maxwell, 1996; Cheng et al., 2022; Indarto et al., 2016; Kang et al., 2022; Lei et al., 2011; Qiutan & Yong, 2019; Tan et al., 2009a; Tan et al., 2020). A key advantage of this method is its reliance on a single parameter – the recession constant (assumed to be time-invariant), which simplifies the employment of this filter. This constant can be readily and reliably determined by analyzing the recession sections of observed streamflow hydrographs (e.g. Tallaksen, 1995). Notably, research has shown that better separation typically occurs when the recession constant value is high (> 0.90) (Indarto et al., 2016; Kang et al., 2022).

Another largely employed RDFs is the Eckhardt's filter (Eckhardt, 2005), a two-parameter model, given as:

$$qbECK_t = \frac{(1 - BFI_{max}) \times a \times qbECK_{t-1} + (1 - a) \times BFI_{max} \times q_t}{1 - a \times BFI_{max}} \quad (3)$$

where BFI_{max} [0,1] is the model parameter (time-invariant), representing the highest BFI that the filter can compute.

The Eckhardt's filter is usually preferred over other RDFs for more accurate baseflow values and versatility across catchment sizes and types, as demonstrated by various studies (Eckhardt, 2008; Gonzales et al., 2009; Helfer et al., 2024; Latuamury et al., 2022; Minea, 2017; Narimani et al., 2023; Shao et al., 2020; Xie et al., 2020). Its main disadvantage, however, is its dependence on two parameters – recession constant and BFI_{max}. BFI_{max} values are often chosen based on hydrogeological characteristics of catchments, with empirical determinations suggesting values between 0.70-0.80 for perennial streams with porous aquifers, 0.50 for ephemeral streams, and 0.20-0.25 for hard rock aquifers (Eckhardt, 2005, 2008). Baseflow estimation is often influenced by this arbitrary selection of BFI_{max}, leading to uncertainties and inaccuracies, particularly because the filter is highly sensitive to this parameter (Eckhardt, 2012; Narimani et al., 2023; Okello et al., 2018; Zhang et al., 2017). Studies highlight the importance of calibrating BFI_{max} against other flow separation methods or tracer-based data, and have demonstrated that site-specific calibration can improve the algorithm's performance significantly (Gonzales et al., 2009; Helfer et al., 2024; Kouanda et al., 2018; Su et al., 2016; Zhang et al., 2013). This need for calibration is further supported by the fact that BFI is influenced by various factors beyond hydrogeology. These include, for example, precipitation and evapotranspiration, and relationships between the two, such as the aridity index (Beck et al., 2013; Haberlandt et al., 2001; Lacey & Grayson, 1998; Mwakalila et al., 2002; Wu et al., 2019; Yao et al., 2021), soil properties such as infiltration, drainage capacity, water storage capacity and hydraulic conductivity (Ahiablame et al., 2013; Beck et al., 2013; Bloomfield et al., 2009; Longobardi & Villani, 2023; Yao et al., 2021), topographic factors such as slope, area, drainage density, altitude (Beck et al., 2013; Haberlandt et al., 2001; Lacey & Grayson, 1998; Mazvimavi et al., 2004; Mehaiguene et al., 2012; Mwakalila et al., 2002), land use and occupation (Lacey & Grayson, 1998; Mazvimavi et al., 2004), and seasonality (Longobardi & Villani,

https://doi.org/10.5194/egusphere-2025-244
Preprint. Discussion started: 26 March 2025

2023; Sun et al., 2023). Therefore, it is essential to calibrate BFI_{max} against other methods and data sources to ensure accurate and reliable baseflow estimation.

The calibration of BFI_{max} can be effectively achieved by leveraging baseflow values derived from tracers and the mass balance equation. Among tracers, dissolved silica (DSi) has emerged as a particularly effective tool for determining baseflow values, as demonstrated in studies such as Helfer et al. (2024) and Gonzales et al. (2009). DSi, a stable and easily detectable product of rock weathering (Asano et al., 2003; Cook, 2015; Kennedy, 1971; Laudon & Slaymaker, 1997; Stewart et al., 2007), offers distinct advantages due to its natural abundance and its ability to differentiate between flow components. Pre-event groundwater ("old water"), influenced by prolonged water-rock interactions, typically exhibits high DSi concentrations (Hendershot et al., 1992; Marçais et al., 2018; Scanlon et al., 2001), while surface runoff and soil interflow (event waters, or "new water") are characterized by much lower levels (Beighley et al., 2005; Hendershot et al., 1992; Scanlon et al., 2001). These contrasting DSi concentrations make it an ideal tracer for distinguishing baseflow from quickflow, thereby enabling the refinement of RDF parameters. During the calibration of BFI_{max}, an objective function can be applied to minimize discrepancies between filter-derived and tracer-derived baseflow values, optimizing the BFI_{max} parameter for improved accuracy (e.g., Helfer et al., 2024; Gonzales et al., 2009).

The Collischonn and Fan (2013) method offers an alternative approach for determining BFI_{max} in scenarios where tracer data is unavailable. This technique relies exclusively on streamflow data and the recession constant and can be easily applied and automated. However, its effectiveness is yet to be confirmed through comparison with tracer-based studies. The method's credibility is currently grounded more in theoretical assumption than in concrete, empirical validation. Additionally, preliminary findings from Helfer et al. (2024) indicate that the method might produce inaccurate baseflow separation outcomes if the recession of interflow is not significantly faster than that of baseflow.

Taking the aforementioned factors into account, the overarching aim of this study is to improve the understanding and knowledge of the calibration and application of three baseflow separation filters. In the context of a small (< 1.2 km^2) rural catchment located in the south of Brazil, the specific objectives are:

1) To calibrate the BFI_{max} and *Beta* parameters for Eckhardt's and Lyne and Hollick's (LH) filters. This calibration will utilize a method that aims to reduce the percentage bias between the baseflow estimates produced by these filters and those obtained from dissolved silica concentration analyses.

2) To assess and contrast the performance of the calibrated Eckhardt's and LH filters alongside the Chapman and Maxwell (CM) filter in generating baseflow hydrographs for the catchment. The evaluation will focus on the hydrographs' shapes, the timing of baseflow peaks, and baseflow to streamflow ratio.

3) To examine the performance of the Eckhardt's and LH filters using an 'event calibration approach'. This method involves determining three distinct BFI_{max} and *Beta* values, each associated with the intensity range of rainfall-runoff events recorded in the study area.

https://doi.org/10.5194/egusphere-2025-244
Preprint. Discussion started: 26 March 2025

2. Methodology

2.1. Study site and data collection

The Arvorezinha catchment is located in Brazil's southern region (**Fig. 1**), at coordinates 28°49'35"S 52°12'30"W. Its drainage area is 1.2 km² and its primary creek – the Lajeado Ferreira - is a perennial stream with an average channel slope of 9%. It is made of two perennial branches, one with a length of 1.5 km, and the other with 1.6 km. The creek joins the Guapore River, which is a tributary of the important Taquari River, within the South Atlantic Hydrographic basin.

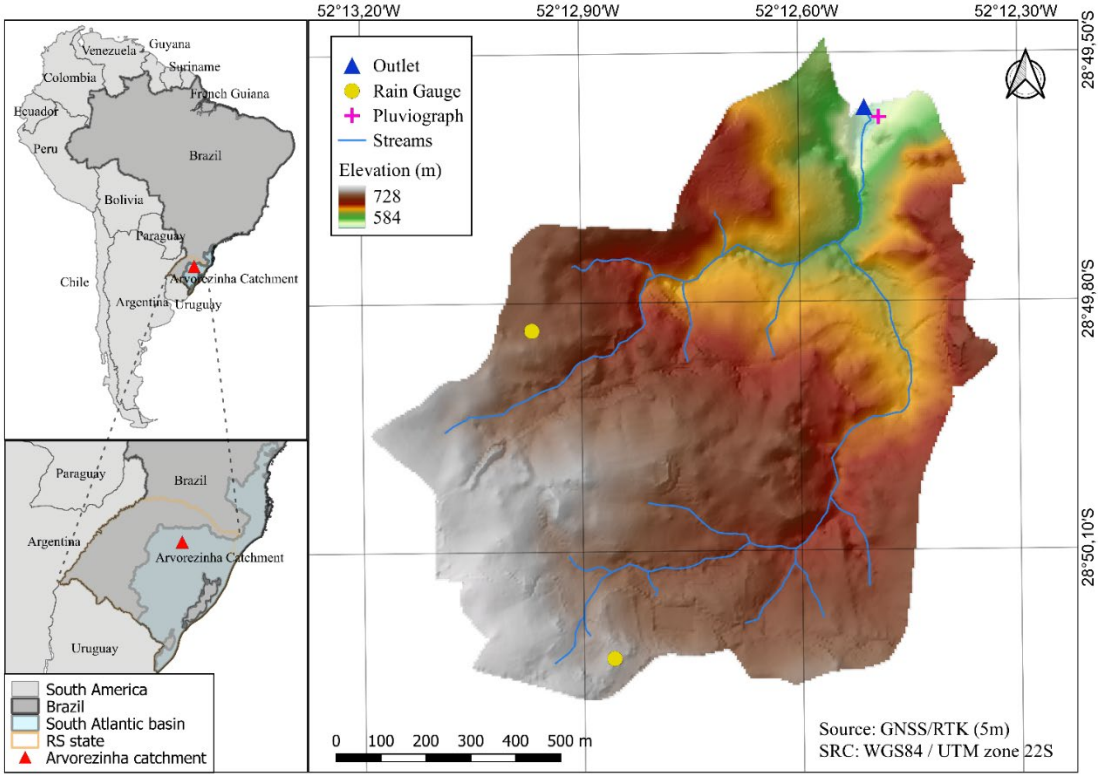

Figure 1: The Arvorezinha catchment and its location in southern Brazil, along with its monitoring network and elevation map. Rain gauges are indicated by yellow circles, the pluviograph, by a pink cross, and the catchment outlet, by a blue triangle.

In terms of geology, the catchment is largely made up of igneous rocks, particularly basalts and rhyodacite, and sits at elevations between 580 and 730 meters above sea level (Tiecher et al., 2017). The terrain in the upper third is relatively gentle, with average slope gradients around 7%, while the middle and lower thirds are more undulated, featuring slopes with higher gradients, sometimes exceeding 15% (de Barros et al., 2014; Minella et al., 2022). Event hydrographs at the catchment outlet typically show lag times varying between 1 to 3 hours (Helfer et al., 2024).

https://doi.org/10.5194/egusphere-2025-244
Preprint. Discussion started: 26 March 2025

The climate in this area is classified as Cf_b (subtropical super-humid with no distinct dry season) by Köppen. Annual precipitation varies between 1250 and 2000 mm. The average annual rainfall from 2002 to 2016 was recorded at 1938 mm by Ramon (2017). Rainfall volumes are evenly distributed throughout the year, but higher rainfall and runoff intensities are observed in spring (September to November).

The soils in the catchment are varied: Acrisols (i.e. 'Argissolos' as per the Brazilian SiBCS Taxonomy System - (Santos et al., 2018)) make up 60% and are primarily found in the upper parts, Leptosols (i.e., 'Neossolos Litólicos') constitute 33% and are located in the lower areas, while Cambisols ('Cambissolos') account for 7% and are interspersed among the other soil types (de Barros et al., 2021; Silva et al., 2021). Leptosols and Cambisols are shallow, with a sandy top layer and no subsurface horizon, lying directly above the igneous bedrock. This structure allows for high infiltration but limited water retention, leading to quick surface and sub-surface runoff, except in areas with fractured bedrock. Acrisols, on the other hand, are deep soils and have a sharp texture change between the A and B horizons, with the B horizon containing more clay and lower infiltration capacity, resulting in slower infiltration and higher moisture retention in the top layer.

The catchment is predominantly rural. Farm sizes range from 5 to 20 hectares, often with low-tech farming practices and diverse land use (de Barros et al., 2021). The main land uses include tobacco farming (13.1%), soybean and maize crops (24%), eucalyptus plantations (34.8%), pastures and grasslands (5.2%), native forests (15.5%), and other varied uses (7.4%) (Ramon, 2017).

The Arvorezinha catchment has been a center for hydrological and erosive process research since 2002, equipped with an extensive hydrological monitoring network to study sediment generation, contamination and soil conservation practices (e.g. de Barros et al., 2021; de Barros et al., 2014; Merten & Minella, 2005; Minella et al., 2022; Ramon et al., 2017; Silva et al., 2021; Tiecher et al., 2021; Uzeika et al., 2012). For precipitation measurement, the setup includes a pluviograph providing 10-minute interval data and two pluviometers recording daily totals. Streamflow data are acquired using a water level encoder and a flume with a 1.829 m throat width. Water level readings, taken every 10 minutes, are converted to flow rates using a stage-discharge rating curve specifically calibrated for this flume.

Relevant to this study, dissolved silica concentrations (DSi) were determined from water samples collected at the catchment's outlet using a USDH-48 sampler (USGS, 1965). Although the overall monitoring of DSi spanned from 2010 to 2015, encompassing over 250 rainfall events with peak flows between 5.0 $l.s^{-1}$ and 5,000 $l.s^{-1}$, intensive DSi and flow monitoring focused on just 15 specific events (listed in **Table 1**). During these selected events, DSi sampling frequency varied from every 30 minutes to 4 hours based on the event characteristics, enabling the identification of crucial baseflow hydrograph points such as the pre-event level, peak, and recession. Detailed methodologies for DSi analysis are documented in the works of de Barros (2016) and de Barros et al. (2021).

https://doi.org/10.5194/egusphere-2025-244
Preprint. Discussion started: 26 March 2025

Table 1: Characteristics of the 15 rainfall-runoff events analyzed in this study for baseflow hydrograph determination using DSi measurements.

Event	Date	Number of DSi samples	Q_{max} ($m^3\ s^{-1}$)	Q_{min} ($l.s^{-1}$)	P_t (mm)	M_i ($mm.h^{-1}$)	D (h)
1	17/07/2011	14	3277.6	54.1	107.7	5.82	18.5
2	01/10/2011	7	56.0	15.1	20.4	6.12	3.3
3	06/07/2012	9	518.4	2.9	105.0	4.63	22.7
4	26/08/2012	4	43.2	7.4	36.1	1.85	19.5
5	09/09/2012	6	35.3	11.8	27.0	5.22	5.2
6	12/03/2013	8	230.8	43.9	32.1	5.35	6.0
7	23/09/2013	6	532.4	31.0	37.1	7.68	4.8
8	26/10/2013	10	445.3	42.9	35.2	8.45	4.2
9	19/03/2014	3	125.1	17.7	34.3	4.79	7.2
10	23/07/2014	13	493.0	26.6	55.2	6.25	8.8
11	07/07/2015	11	535.1	80.4	48.7	2.21	22.0
12	12/07/2015	6	195.8	48.1	15.4	2.71	5.7
13	13/07/2015	15	582.7	78.8	57.2	5.20	11.0
14	23/07/2014	6	998.0	265.5	28.1	4.97	5.7
15	15/07/2015	3	353.2	189.6	12.1	1.54	7.8

Notes: Q_{max} refers to the peak streamflow observed within the event, captured in a 10-min interval dataset, while Q_{min} reflects the lowest streamflow recorded. P_t denotes the total rainfall throughout the event, M_i represents the average rainfall intensity during that period, and D indicates the duration of the event, measured in hours.

The estimation of baseflow rates from DSi concentrations was carried out using a mass balance approach, represented by the following equation:

$$q \times DSi_q = qb_{DSi} \times DSi_{qb} + qs \times DSi_{qs} \quad (4)$$

where DSi_q corresponds to the measured DSi concentration in the observed streamflow (q), DSi_{qb} represents the concentration of DSi associated with (qb_{DSi}), and DSi_{qs} is the DSi concentration in quickflow (qs) during rainfall events.

An important assumption in this tracer-based separation method is that quickflow (qs) carries an insignificant amount of DSi, meaning $DSi_{qs} \approx 0$ (de Barros, 2016; Gonzales et al., 2009). This assumption is justified by two key considerations. Firstly, since quickflow primarily originates from precipitation, its DSi content is minimal (Beighley et al., 2005; de Barros, 2016; Hugenschmidt et al., 2014; Rodhe, 1998; Wels et al., 1991). Secondly, quickflow has limited interaction with silica-enriched sediments, unlike groundwater, which undergoes prolonged contact along deeper subsurface pathways (Hendershot et al., 1992; Rodhe, 1998; Wels et al., 1991). Given this, the mass balance equation simplifies to: $qb_{DSi} = q \times \frac{DSi_q}{DSi_{qb}}$.

The DSi concentration corresponding to baseflow (DSi_{qb}) was determined from streamflow samples collected after extended dry periods, during which streamflow was assumed to be entirely sustained by groundwater (Beighley et al., 2005; Gonzales

https://doi.org/10.5194/egusphere-2025-244
Preprint. Discussion started: 26 March 2025

et al., 2009; Wels et al., 1991). This concentration exhibited stability over time (de Barros, 2016), making it a reliable indicator of the DSi signature of groundwater and, consequently, baseflow in the catchment.

2.2. Recession constant – a parameter for the Eckhardt's and CM filters

Prior to calibrating the filters using the baseflow values derived from DSi, the methodology involved calculating the recession constant, a. The recession constant is required for both the CM and Eckhardt's filters (see Equations 2 and 3). The calculation of a involved establishing a linear relationship between the flow rates during recession phases at time t, and the flow rates at the next time step, $t+1$, following the methodology proposed by Eckhardt (2008) and Vogel and Kroll (1996), as represented by **Eq. 5**:

$$qb_{t+1} = a \times qb_t \quad (5)$$

To determine the recession constant, data from 254 hydrographs recorded between 2010 and 2015 at 10-minute intervals were analyzed. The onset of the recession phase was identified as occurring no sooner than two hours after the most recent peak flow, ensuring that the influence of quickflow was minimized. Additionally, a sustained decline in flow for a minimum duration of 1.5 hours was required. Once these criteria were satisfied, the flow rate (q) was assumed to be representative of baseflow (qb). The recession constant was then estimated by plotting qb_{t+1} against qb_t and determining the slope of the regression line that best fit the data, with the constraint that it passed through the origin.

2.3. Optimized BFI_{max} (Eckhardt's filter) and *Beta* (LH filter) parameters

The calibration process for the BFI_{max} and *Beta* parameters, used in the Eckhardt's and LH filters respectively, involved utilizing an objective function to determine their optimal values for the catchment across all 15 events. The goal was to identify BFI_{max} and *Beta* values that would minimize the Percent Bias (*PBias*) error. This error measured the discrepancy between the baseflow model estimates (qb) generated by the filters and the actual observed baseflow values (qb_{DSi}) derived from DSi data for the 15 events. *PBias* represents the average bias of the model outputs, indicating whether they tend to under or overestimate the observed values. A *PBias* of 0% indicates perfect agreement, positive values imply overestimation, and negative values indicate underestimation.

A computational algorithm was written to iteratively refine the BFI_{max} and *Beta* values, searching within their respective limits ($0.001 \leq BFI_{max} \leq 0.999$ and $0.900 \leq Beta \leq 0.999$) to minimize the *PBias* value, aiming to bring it as close to zero as possible. The *PBias* was computed using **Eq. 6**:

$$PBias = 100 \times \frac{\sum_{i=1}^{N}(qb_i - qb_{DSi_i})}{\sum_{i=1}^{N} qb_{DSi_i}} \quad (6)$$

where qb_i is the modelled baseflow computed by the filters (*qbECK* or *qbLH*, as per Equations 1 and 3), and qb_{DSi_i} is the silica-derived baseflow from the mass balance equation (**Eq. 4**).

https://doi.org/10.5194/egusphere-2025-244
Preprint. Discussion started: 26 March 2025

2.4. Optimized filters: Application and comparison

After determining the optimal BFI_{max} and *Beta* parameters, the Eckhardt's and LH filters (**Eq. 1** and **Eq. 3**), alongside the CM filter (**Eq. 2**), were employed to separate baseflow from the 15 analyzed rainfall-runoff events (referenced in **Table 1**). After the separation, various performance metrics such as the Nash-Sutcliffe Efficiency (*NSE*, **Eq. 7**), Kling-Gupta Efficiency (*KGE*, **Eq. 8**), and Root Mean Square Deviation (*RSMD*, **Eq. 9**) were calculated using modelled and silica-derived baseflows to evaluate the effectiveness of the models.

The *NSE* (**Eq. 7**) quantifies the proportion of the residual variance relative to the variance of the observed data, with its values ranging from minus infinity to 1 (Nash & Sutcliffe, 1970). For the model performance to be considered at least minimally acceptable, *NSE* values should exceed zero (Gupta et al., 1999), whereas negative values indicate unsatisfactory performance (Knoben et al., 2019). An *NSE* of 1 means a perfect agreement between the observed and modeled values. Generally, an *NSE* greater than 0.5 is deemed "good" (Partington et al., 2011; Su et al., 2016), and an *NSE* above 0.8 is regarded as "very good" or "excellent" for daily flow assessments (Gupta et al., 1999; Moriasi et al., 2007; Moriasi et al., 2015).

$$NSE = 1 - \frac{\sum_{i=1}^{N}\left(qb_{DSi_i} - qb_i\right)^2}{\sum_{i=1}^{N}\left(qb_{DSi_i} - mean\left(qb_{DSi_i}\right)\right)} \quad (7)$$

The *KGE* metric, introduced by Gupta et al. (2009), is used to evaluate a model's capability to accurately reflect the observed data's mean, variability, and correlation. Like the *NSE*, *KGE* values can be between negative infinity to 1, where a value of 1 denotes a perfect match between the observed and modeled data. According to Knoben et al. (2019), a *KGE* value greater than -0.41 suggests that using the model's predictions of baseflow is better than simply using a time-constant baseflow. Consequently, *KGE* values below -0.41 are deemed inadequate or "unwanted".

$$KGE = 1 - \sqrt{(r-1)^2 + (\gamma - 1)^2 + (\lambda - 1)^2} \quad (8)$$

where r is the Pearson correlation coefficient, representing the strength of the linear relationship between observed and modeled values; γ denotes the ratio of the standard deviation of the modeled data to that of the observed data; and λ is the ratio of the mean of the modeled data to the mean of the observed data.

The *RMSD* metric, denoted in **Eq. 9**, quantifies the standard deviation of the residuals, serving as a consolidated measure of the magnitude of errors across model predictions. The *RMSD* values range from 0 to positive infinity, where lower values denote improved model accuracy (with a perfect match indicated by 0). In this research, a normalized version of *RMSD* (*NRMSD*, shown in **Eq. 10**), calculated by dividing the *RMSD* by the observed baseflows' range, was employed to standardize comparisons across events. Lower *NRMSD* values (in percentage) indicate lesser residual variance. For the purposes of this study, *NRMSD* values below 20% were deemed indicative of satisfactory model performance.

https://doi.org/10.5194/egusphere-2025-244
Preprint. Discussion started: 26 March 2025

$$RMSD = \left(\frac{\sum_{i=1}^{N}(qb_i - qb_{DSi_i})^2}{N}\right)^{\frac{1}{2}} \quad (9)$$

$$NRMSD = \frac{RMSD}{qb_{DSi(max)} - qb_{DSi(min)}} \quad (10)$$

2.5. Event magnitude classification

One of the objectives of this study was the calibration of the BFI_{max} and *Beta* parameters (Eckhardt's and LH filters, respectively) as a function of event magnitude. This calibration aimed to understand how the parameter values varied in response to events of differing intensities within the catchment. Before implementing this calibration, it was necessary to develop a method for classifying the events by their magnitude.

We determined three classes based on the average recurrence intervals (ARI) of the precipitation events monitored in this study (**Table 1**). The classification strategy consisted of separating the hydrographs from precipitation events with ARI less than 0.33 years, between 0.33 and 2 years, and above 2 years. This classification is because ARI > 2 years is commonly used for small hydraulic works and represents extreme values. An ARI of 0.33 can be a divider of medium and small events as it represents an event magnitude that occurs up to three times a year. It is important to highlight that the monitoring period was only 2010 to 2015, which did not allow for a statistical projection of flow and association with their ARIs. Therefore, we established this classification subjectively.

Therefore, the maximum flows (Q_{max}) produced in the 254 precipitation and flow events during the monitoring period 2010 to 2015 were grouped for the respective precipitation classes with ARI < 0.33 year (low magnitude), 0.33 ≤ ARI ≤ 2 years (medium magnitude), ARI ≥ 2 years (high magnitude). The ARI of the 15 rainfall events was determined using the empirical equation developed by Bell (1969) with parameters determined for the southern region of Brazil by Basso et al. (2019). The precipitation with a duration of one day and ARI = 10 years (a parameter required for the ARI equation) was 133.48 mm obtained through the Gumbel distribution of historical (1951-2012) rainfall series provided by the Brazilian National Water Agency, gauge station code 2852014, located at latitude -28.93 and longitude -52.13, about 12 km from the study area.

2.6. Optimized BFI_{max} (Eckhardt's filter) and *Beta* (LH filter) parameters per event magnitude

Following the categorization of the 15 monitored events into the three above-mentioned event magnitude classes, the calibration of the BFI_{max} and *Beta* parameters was conducted using the methodology outlined in the general calibration process (**Section 2.3**). However, the optimization algorithm was executed separately for each of the three event categories, resulting in three distinct calibrations for each filter. The objective was to achieve three sets of BFI_{max} and *Beta* values, one for each event class, that would reduce the *PBias* error between the baseflow calculated by the filters and the actual observed baseflow obtained from DSi data.

https://doi.org/10.5194/egusphere-2025-244
Preprint. Discussion started: 26 March 2025

2.7. Optimized filters with event-based calibration: Application and comparison

After the optimization of the BFI_{max} and *Beta* parameters for each event magnitude class, the Eckhardt's and LH filters, adjusted with these new parameters, were applied to determine the baseflow hydrographs for the 15 rainfall-runoff events. After this separation, evaluation metrics, including *NSE*, *KGE*, and *NRMSD,* were calculated. These metrics facilitated a comparative analysis between the general calibration and the event-specific calibration processes, as well as a comparison among the three studied filters. This comparative analysis included examining the hydrograph shape, the timing of the baseflow peak, and the baseflow to total streamflow ratio, alongside a detailed review of similar values reported in the literature for catchments with comparable characteristics.

3. Results and Discussion

3.1. Recession constant – a parameter for the Eckhardt's and CM filters

The linear regression analysis applied to 254 rainfall-runoff events occurring during the monitoring period (2010-2015) at the Arvorezinha catchment resulted in a recession constant of 0.952, consistent across all hydrographs, regardless of magnitude. This consistency was expected, as such parameter is largely determined by the catchment's inherent features like topography, drainage, soil type, and geology (Fetter, 2001).

Baseflow recession rates typically range from 0.930 to 0.995 (Jain, 2011), positioning a 0.952 value as indicative of rapid baseflow recession, corresponding to a decay rate of approximately 0.05 day^{-1}. The steep catchment slopes, high soil permeability, and basaltic geology explain this rapid recession in the Arvorezinha catchment. Additionally, the value of 0.952 is in line with Beck et al. (2013) and Santarosa et al. (2023), who reported similar, rapid recession constants across different Brazilian climates and catchment sizes, confirming the influence of regional geophysical characteristics on baseflow recession rates. The recession constant 0.952, found for the Arvorezinha catchment, was deemed adequate, and it was then used as an input parameter in the Eckhardt's and CM filters.

3.2. Optimized BFI_{max} (Eckhardt's filter) and *Beta* (LH filter) parameters

The optimization process aiming at minimizing the *PBias* between modeled and observed baseflow values (derived from DSi) for 15 events, resulted in an optimal BFI_{max} value of 0.653 for the Eckhardt's filter and 0.965 for the *Beta* parameter of the LH filter. For both models, the optimization effectively achieved a *PBias* close to 0.

The determined BFI_{max} value of 0.653 is in close agreement with findings from studies on small catchments, such as Zhang et al. (2013), who found a BFI_{max} of 0.62 for a 14.5 km² catchment with shallow soils, and Stewart (2015), who reported a BFI_{max} of 0.69 for a 2.18 km² catchment with varied soil depths (0.5 m to 3 m). This value also aligns with the results by Eckhardt (2008) across 65 U.S. catchments, and by Okello et al. (2018) for catchments in South Africa of medium size. A BFI_{max} value of 0.653 indicates that the model assumes the maximum long-term baseflow contribution to total flow to be 65.3%. It is

https://doi.org/10.5194/egusphere-2025-244
Preprint. Discussion started: 26 March 2025

important to note, however, that this value is significantly larger than the arbitrary value of 0.25 suggested by Eckhardt (2005) for catchments with hydrogeological characteristics similar to the one used in our study.

The optimum *Beta* parameter of 0.965 diverges from the commonly referenced value of 0.925 reported in the literature (Arnold et al., 1995; Nathan & McMahon, 1990). This conventional value is often adopted globally in the absence of specific catchment data; however, there is an indication that a larger value usually yields better separation (CSIRO & SKM, 2010; Ladson et al., 2013; Li et al., 2013; Zhang et al., 2017), which is in alignment with the finding of our study.

3.3. Optimized filters: Application and comparison

Figure 2 shows the results of the three separation methods investigated in this study. As described in the previous section, the formulas of Eckhardt (**Eq. 3**) and LH (**Eq. 1**) were calibrated for the parameters BFI_{max} and *Beta*, respectively, using the *PBias* minimization approach, before their application in the baseflow separation of the 15 events examined in this study (referenced in **Table 1**). Conversely, the CM method was implemented directly via **Eq. 2**, devoid of any calibration requirement for fitting parameters. This method relies exclusively on the recession constant, a parameter considered constant for the catchment.

Visually inspecting **Fig. 2**, it can be seen that the Eckhardt's (dark blue) and the CM (cyan) models yielded plausible baseflow hydrographs, both in terms of their shape and the timing of their peaks. These models accurately follow the overall smoothness observed in the streamflow hydrographs and exhibit a logical delayed peak when compared to the streamflow hydrograph's peak. Specifically, the baseflow peak occurs, on average, 1.5 hours later for the Eckhardt's filter and 1.8 hours later for the CM filter, in relation to the streamflow peak (noting that the second peak was considered for events featuring dual peaks). In contrast, the LH model's baseflows increase more gradually, reaching their peak near the end of the direct runoff hydrographs and thus demonstrating a significantly longer delay in peak timing than the other two methods, with an average delay of 4.4 hours across the 15 events. It is also noteworthy that the baseflow hydrographs from the LH method converge with the streamflow hydrographs much before the rainfall-runoff event ends, a behavior that appears unrealistic.

Table 2 shows the performance indicators *PBias, NSE, KGE,* and *NRMSD* computed for the three methods. These metrics were calculated by comparing modelled baseflows with baseflow values derived from DSi data (black dots in **Fig. 2**). For the Eckhardt's filter, the performance metrics were: $PBias \approx 0$, $NSE = 0.85$, $KGE = 0.76$, and $NRMSD = 7.5\%$, all of which fall within acceptable ranges for hydrological modeling. For the LH method, the metrics were: $PBias \approx 0$, $NSE = 0.79$, $KGE = 0.74$, and $NRMSD = 8.9\%$, indicating satisfactory performance as well. However, the CM model presented $PBias = -28\%$, $NSE = 0.86$, $KGE = 0.70$, and $NRMSD = 7.2\%$, indicating a significant underestimation of baseflows highlighted by the substantial negative *PBias*, exceeding the acceptable limit of +/- 25% set in this study. This result highlights a limitation of the CM method – its inability to be calibrated due to the lack of adjustable parameters, relying solely on the recession constant, which is typically considered an invariant characteristic of the catchment. Yet, some scholars suggest that this constant may vary, proposing a potential for calibration and improvement of the CM model's baseflow separation. Exploring this possibility,

https://doi.org/10.5194/egusphere-2025-244
Preprint. Discussion started: 26 March 2025

355 particularly given the CM method's accurate representation of baseflow shape and timing, warrants further research. This could offer a path to enhance the CM model's performance, addressing its current shortfall in accurately estimating baseflow.

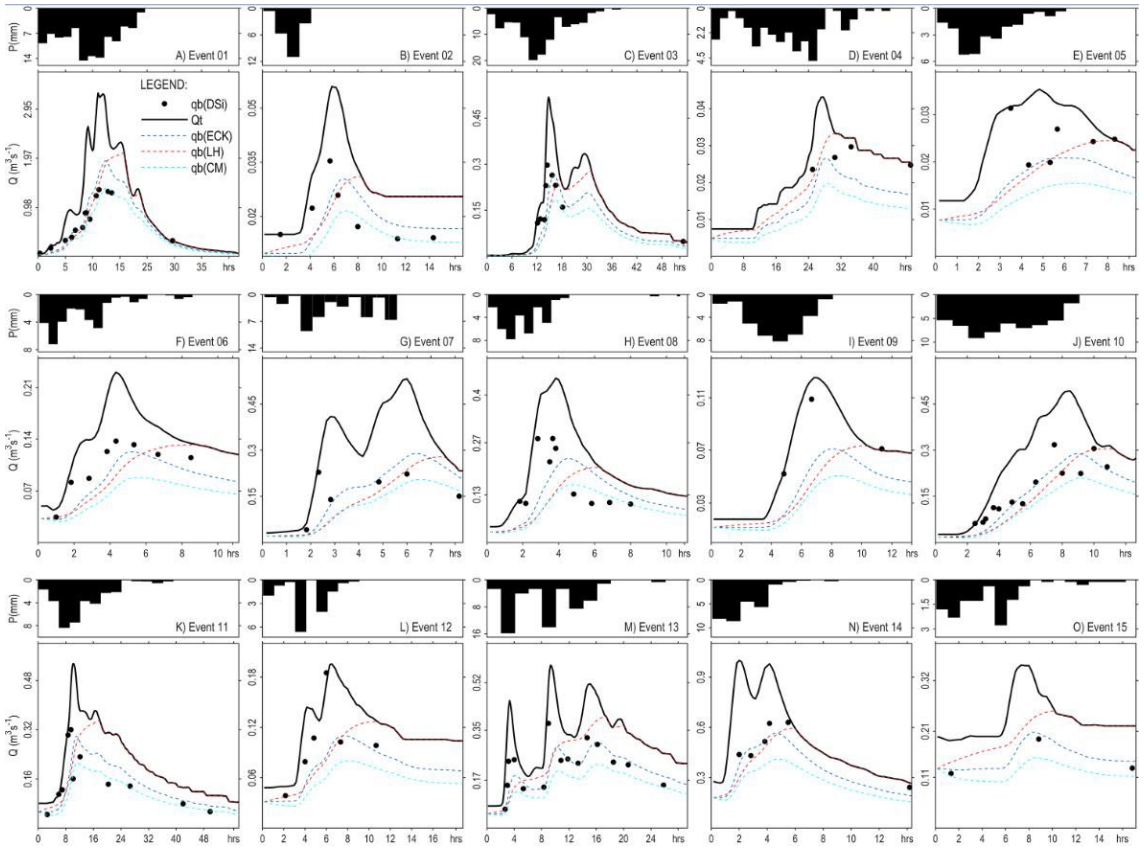

Figure 2. Comparison of baseflow separation techniques on 15 events in the Arvorezinha catchment (Brazil): total streamflow (*Qt*) as solid black curves; silica-derived baseflow (*qb(DSi)*) as black dots; Eckhardt's filter baseflow (*qb(ECK)*) 360 in blue dotted lines; LH filter baseflow (*qb(LH)*) in red dotted lines; and CM filter baseflow (*qb(CM)*) in cyan dotted lines.

Table 2. Error metrics comparison for modeled *versus* observed (DSi-derived) baseflows considering 15 events in combination, and three separation methods: Eckhardt's filter (a = 0.952, BFI_{max} = 0.653), CM filter (a = 0.952), and LH filter (β = 0.965). The criteria for acceptable model performance were defined as *NSE* > 0.5, *KGE* > -0.41, *NRMSD* < 10% and *PBias* < +/- 25%

Filter	*PBias* (%)	*NSE*	*KGE*	*NRMSD* (%)
Eckhardt	< 0.05	0.85	0.76	7.5
CM	-28	0.86	0.70	7.2
LH	< 0.05	0.79	0.74	8.9

https://doi.org/10.5194/egusphere-2025-244
Preprint. Discussion started: 26 March 2025

In terms of volume, the Eckhardt's filter showed higher volumes than the CM model. The LH model resulted in overall higher baseflow volumes than the other two models. For model comparison of volumes, we assessed the baseflow to streamflow ratios (*BF* ratio = Total Baseflow Volume / Total Streamflow Volume) for each model over 15 rainfall-runoff events, with the findings presented in **Table 3**.

Table 3. Comparative analysis of average *BF* ratios for the Arvorezinha Catchment (1.2 km²) in the South of Brazil across 15 rainfall-runoff events using various baseflow separation methods, alongside literature reference values.

Separation Method	*BF* ratio (15 rainfall-runoff events)	Reference values of *BF* ratios for catchments similar to the study area or catchments located in the south of Brazil
Mass balance (DSi-derived baseflows)	66% CV = 0.19	• 60-72% for rhyodacite catchments in Australia (Lacey & Grayson, 1998) • 67-91% for basalt catchments in Australia (Lacey & Grayson, 1998) • 50-70% for basalt catchments in the same hydrographic region in Brazil (Chagas et al., 2020) • 54-65% for catchments overlying igneous aquifers in southeastern Brazil (Santarosa et al., 2023) • 60-64% for small rural catchments overlying igneous aquifers in Kenya (Mugo & Sharma, 1999) • 61% average *BF* ratio for six small rural catchments over granite and gneiss in Southeastern Brazil (Costa & Bacellar, 2009) • 63% for catchments in Cf climate regions (Beck et al., 2013) • >60% for catchments in the south of Brazil (Tan et al., 2020) • >65% for catchments underlain with basalt and granite in Tanzania (Mwakalila et al., 2002) • 50-70% is the predominant *BF* ratio in an analysis of 1815 undisturbed catchments in the USA. It occurs in 50% of the catchments (Xie et al., 2020)
Eckhardt's Filter (calibrated) (a = 0.952; BFI_{max} = 0.653)	64% CV = 0.04	
CM Filter (a = 0.952)	49% CV = 0.06	
LH Filter (calibrated) (β= 0.965)	75% CV = 0.15	

The *BF* ratios were determined to be 64%, 49%, and 75% for the Eckhardt's, CM, and LH filters, respectively. The *BF* ratio based on baseflows calculated from DSi was 66%, positioning the Eckhardt's filter as the most aligned with observed data. Moreover, the Eckhardt's filter exhibited the most consistent performance across the 15 events, demonstrating the lowest variability with a coefficient of variation (CV) at 0.04, as shown in **Table 3**. This consistency is crucial for accurately reflecting catchment conditions, as highlighted by Nathan and Mcmahon (1990). Furthermore, the results obtained from the Eckhardt's filter are closely aligned with several findings reported in the literature. Lacey and Grayson (1998) identified a notable trend of higher *BF* ratios in catchments underlain by igneous rocks, such as basalt and rhyodacite, compared to those underlain by sedimentary and metamorphic rocks. Their study, which included 23 catchments underlain by basalt and/or rhyodacite (reflecting the geological composition of the study catchment), reported *BF* ratios of 66% for rhyodacite and 79% for basalt, compared to an average of 54% across 114 catchments with diverse geological formation. They attributed the high *BF* ratios in igneous rock catchments to high primary porosity and the presence of fractures, which enhances groundwater recharge, storage capacity, and the formation of deep, permeable soils. A similar trend was reported by Mwakalila et al. (2002) in which larger *BFI* values were found for catchments underlain with granites and basalt in an examination of 12 catchments ranging

https://doi.org/10.5194/egusphere-2025-244
Preprint. Discussion started: 26 March 2025

from 66 to 2930 km^2 in semi-arid environments of Tanzania. Such characteristics are consistent with those of the Arvorezinha catchment, supporting the observed high baseflow proportion. Therefore, the *BF* ratios from DSi-based baseflows, along with those obtained from Eckhardt's and LH filters in the Arvorezinha catchment, were in realistic agreement with expectations, while the CM filter's derived *BF* ratio appeared to be an outlier. Table 3 further includes comparative *BF* values from the literature for catchments analogous to the one under study, providing a broader context for our findings.

Therefore, considering shape, peak timing, magnitude and *BF* ratios, the Eckhardt's filter emerges as the most accurate for baseflow separation in the Arvorezinha catchment. The superior performance of the Eckhardt's filter over the LH and the CM models matches the results reported by Xie et al. (2020), who evaluated nine separation methods in 1815 catchments in the USA, demonstrating higher *NSE* and *KGE* values for the Eckhardt's filter. Similarly, Gonzales et al. (2009) reached a comparable conclusion when they evaluated seven non-tracer-based separation methods against baseflow estimations derived from a tracer-based approach in a lowland catchment in the Netherlands, further reinforcing the effectiveness of the Eckhardt's filter.

Figure 3 illustrates the relationship between modeled and observed baseflow values for the three filters. For the Eckhardt's and LH filters, it can be seen that low flows are underestimated, and high flows are overestimated. A more favorable agreement is noted for mid-range flows. These results were expected since this is a direct consequence of adjusting the BFI_{max} and *Beta* parameters to reduce the average discrepancy between observed and modeled values. As such, this process leads to the models balancing underestimated values through overestimating values in other instances, and vice versa. For the CM model, the flows were generally underestimated.

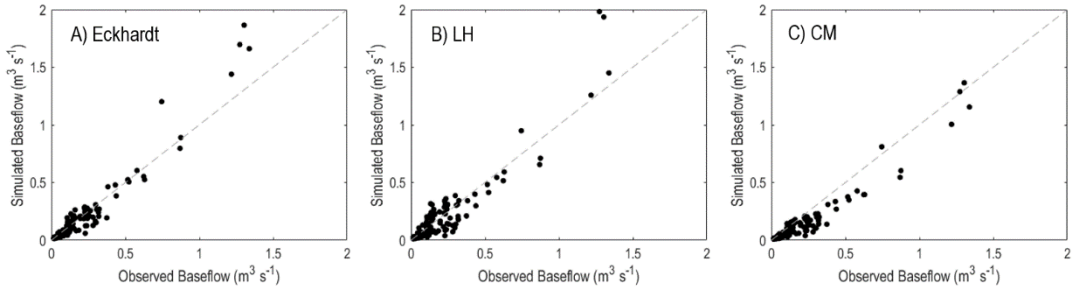

Figure 3: Scatter plot comparing modeled baseflow values against observed values derived from DSi, with the grey dashed line representing the 1:1 line. For the Eckhardt (A) and LH (B) models, the plots show the calibrated models' trend to overestimate higher baseflows and underestimate lower baseflows, a predictable result from the optimization method employed during calibration. The CM model (C) consistently underestimated the baseflow values.

Despite the quality indicators indicating a satisfactory match between the modeled and observed baseflows (**Table 2**), pinpointing a *Beta* value of 0.952 and a BFI_{max} value of 0.653 as the optimal parameters for this specific catchment, discrepancies become evident upon examining data from separate events (refer to **Tables 4** and **5**), suggesting that

https://doi.org/10.5194/egusphere-2025-244
Preprint. Discussion started: 26 March 2025

410 improvements could be achieved with event-specific calibration. **Tables 4** and **5** show that most events did not meet all the quality indicators criteria simultaneously. This issue reveals the calibrated models' challenge in precisely capturing baseflow in some cases, implying that a calibration process designed for each event or event of similar sizes might offer more accurate modeling than a generalized approach.

Table 4. Error metrics comparison for observed versus modeled baseflows across 15 events, utilizing the calibrated
415 **Eckhardt's filter** (a = 0.952, BFI_{max} = 0.653). The criteria for acceptable model performance were defined as *NSE* > 0.50, *KGE* > -0.41, *NRMSD* < 10% and *PBias* < +/- 25%

Event	Q_{max} (l.s^{-1})	DSi samples	*PBias* (%)	*NSE*	*KGE*	*NRMSD* (%)	*BF ratio*
1	3277.6	14	17.7	0.66	0.55	19.6	0.65
2	56.0	7	-3.8	0.10	0.51	32.4	0.64
3	518.4	9	-21.3	0.31	0.69	26.3	0.65
4	43.2	4	-24.6	-4.50	0.52	111.1	0.64
5	35.3	6	-22.3	-2.41	-0.65	63.0	0.61
6	230.8	8	-19.5	0.45	0.79	23.2	0.61
7	532.4	6	-7.5	-0.49	0.38	41.7	0.56
8	445.3	10	-13.3	-0.23	0.26	46.7	0.62
9	125.1	3	-43.9	-1.37	0.44	64.0	0.61
10	493.0	13	-9.6	0.77	0.83	15.9	0.59
11	535.1	11	-4.2	0.33	0.61	26.3	0.65
12	195.8	6	-27.7	-0.04	0.37	30.5	0.63
13	582.7	15	-10.1	0.33	0.65	20.4	0.64
14	998.0	6	-8.5	0.76	0.87	16.7	0.65
15	353.2	3	8.03	0.86	0.92	16.3	0.65
All events combined		121	< 0.05	0.85	0.74	7.5	0.64

Table 5. Error metrics comparison for observed versus modeled baseflows across 15 events, utilizing the calibrated **LH filter** (β= 0.965). The criteria for acceptable model performance were defined as *NSE* > 0.50, *KGE* > -0.41, *NRMSD* < 10% and *PBias* < +/- 25%

Event	Q_{max} (l.s^{-1})	DSi samples	*PBias* (%)	*NSE*	*KGE*	*NRMSD* (%)	*BF ratio*
1	3277.6	14	8.7	0.58	0.52	21.7	0.71
2	56.0	7	8.3	-0.89	-0.03	47.1	0.79
3	518.4	9	-34.8	-0.48	0.43	38.5	0.78
4	43.2	4	6.3	-1.47	-0.17	59.6	0.88
5	35.3	6	-16.8	-2.28	-0.28	61.9	0.67
6	230.8	8	-18.9	0.08	0.67	30.0	0.69
7	532.4	6	-21.5	-1.00	0.29	48.4	0.50
8	445.3	10	-25.4	-1.17	-0.24	61.9	0.63
9	125.1	3	-42.1	-2.10	0.20	73.2	0.67
10	493.0	13	-15.4	0.61	0.69	20.9	0.60
11	535.1	11	9.2	-0.18	0.38	35.0	0.88
12	195.8	6	-23.7	-0.25	0.29	33.4	0.79

https://doi.org/10.5194/egusphere-2025-244
Preprint. Discussion started: 26 March 2025

13	582.7	15	7.7	-0.49	0.39	30.3	0.82
14	998.0	6	-11.3	0.66	0.81	19.9	0.74
15	353.2	3	38.2	-2.66	0.44	84.1	0.85
All events combined		121	< 0.05	0.79	0.76	8.9	0.75

3.4. Event magnitude classification

The violin diagrams in **Fig. 4** display the distribution of the peak flow rates from 254 rainfall-runoff events observed during the monitoring period (2010-2015) into the classes 'low' (precipitation with ARI < 0.33 year), 'medium' (precipitation with 0.33 ≤ ARI ≤ 2 years), and 'high' (precipitation with ARI > 2 years). The stream flow rate thresholds to distinguish the three classes were selected based on the interquartile ranges of the three classes. As such, hydrographs with peak flow rates < 250 ℓ s^{-1} (= third quartile of the first class) were classified as 'low' magnitude. Hydrographs with peak flow rates between 250 ℓ s^{-1} and 1000 ℓ s^{-1} (= third quartile of the second class) were classified as 'medium' magnitude. Hydrographs with peak flow rates higher than 1000 ℓ s^{-1} were classified as 'high' magnitude.

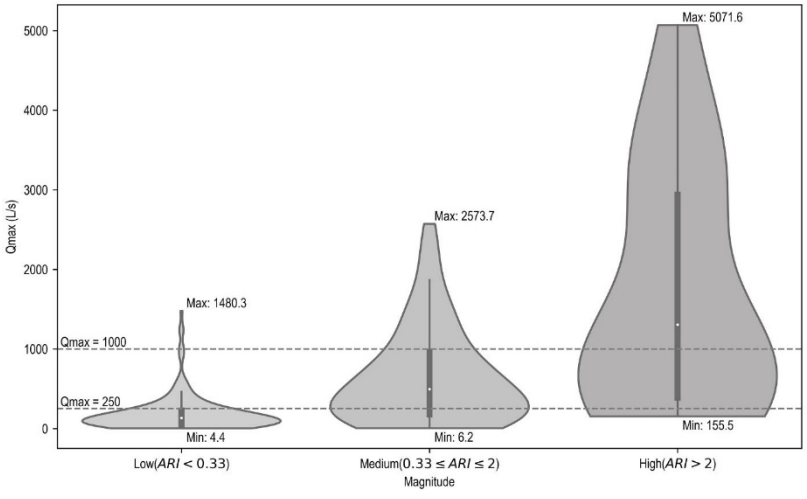

Figure 4: Distribution of peak flow rates from 254 rainfall-runoff events observed during the monitoring period (2010-2015) into the classes 'low', 'medium', and 'high' magnitudes.

The results of the distribution of events within each class of event magnitude, excluding the outliers, is presented in **Table 6**. The number of events observed in each class over the six-year data series period (2010 to 2015) is also shown, highlighting a higher occurrence of low-magnitude events (134) compared to medium (61) and high magnitudes (33).

https://doi.org/10.5194/egusphere-2025-244
Preprint. Discussion started: 26 March 2025

Table 6: Distribution of the 15 monitored rainfall-runoff into the classes 'low', 'medium', and 'high' magnitudes.

Class	Peak magnitude	N° of events between 2010 and 2015[1]	DSi events[2]	DSi samples
Low	< 250 ℓs^{-1}	134	2,4,5,6,9,12	34
Medium	250 - 1000 ℓs^{-1}	61	3,7,8,10,11,13,14,15	73
High	> 1000 ℓs^{-1}	33	1	14

[1] Denotes the total number of events observed in the period 2010-2015. [2] Denotes the events used for analysis due to the availability of DSi data, as listed in **Table 1**.

3.5. Optimized *BFI$_{max}$* (Eckhardt's filter) and *Beta* (LH filter) parameters per event magnitude

The optimization process, aimed at reducing the *PBias* between modeled and observed baseflow values (derived from DSi) for each event magnitude category listed in **Table 6**, yielded three significantly distinct *BFI$_{max}$* values:

- 0.809 for 'low' magnitude events;
- 0.701 for 'medium' magnitude events; and
- 0.576 for 'high' magnitude events.

These values show a notable deviation from the average *BFI$_{max}$* value of 0.653 established for the catchment, suggesting the *BFI$_{max}$* parameter's sensitivity to the magnitude of rainfall-runoff events. The calibration for each event category achieved *PBias* values near zero. Like the general calibration, the *BFI$_{max}$* values derived per event magnitude also exceeded the arbitrary value of 0.25 recommended by Eckhardt (2005) for catchments of hydrogeological characteristics like the Arvorezinha's, supporting the study's hypothesis that events of low magnitude align better with higher *BFI$_{max}$* values, whereas those of high magnitude align better with lower values. This observation is consistent with findings by Minea (2017) and Okello et al. (2018), who reported higher *BFI$_{max}$* values during low-flow (dry) seasons and lower values during high-flow (wet) seasons. Zhang et al. (2013) also noted a similar trend with larger baseflow indexes in dry seasons compared to wet seasons in a Canadian catchment.

For the *Beta* parameter of the LH filter, optimal values were identified as:

- 0.921 for 'low' magnitude;
- 0.957 for 'medium' magnitude; and
- 0.970 for 'high' magnitude events.

These values diverge from the catchment's average *Beta* value of 0.965, indicating that this parameter is also influenced by event magnitude. Interestingly, only the calibration for 'low' magnitude events aligns with the widely recognized standard value of 0.925 referenced in the literature (Arnold & Allen, 1999; Arnold et al., 1995; Lyne & Hollick, 1979; Nathan & Mcmahon, 1990). The values determined for 'medium' and 'high' magnitude events exceed this benchmark, falling outside the commonly accepted range of 0.90 to 0.95 (Nathan & McMahon, 1990). Additionally, the *Beta* value for 'medium' magnitude events (0.957) is closely aligned with the recession constant. This finding supports the approach of using the recession constant as the most suitable parameter for calibration, a strategy endorsed by numerous researchers (e.g. Eckhardt,

https://doi.org/10.5194/egusphere-2025-244
Preprint. Discussion started: 26 March 2025

2005; Tan et al., 2009b; Zhang et al., 2017; Mugo & Sharma, 1999). The highest *Beta* value identified in this study (0.970) aligns with findings by SKM and CSIRO (2012), as cited by Ladson et al. (2013), where a *Beta* value of 0.98 was deemed more appropriate for Australian catchments analyzed using tracer-based baseflow measurements. It is important to recognize the inverse relationship between the *Beta* parameter and the *BF* ratio; lower *Beta* values lead to higher *BF* ratios and vice versa. This result logically follows, as lower flows typically have a larger baseflow contribution, reflected in the lower *Beta* values for low-magnitude events. Thus, the study concludes that lower *Beta* values are more suitable for low-magnitude events, while higher values are more apt for high-magnitude events.

3.6. Optimized filters with event-based calibration: Application and comparison

Figure 5 shows the results of the three separation methods analyzed in this study, in which the Eckhardt's and the LH filters underwent calibration for BFI_{max} and *Beta* parameters based on event magnitude. The method CM, on the other hand, was applied directly using **Eq. 2**, since this method does not have a fitting parameter that can be calibrated.

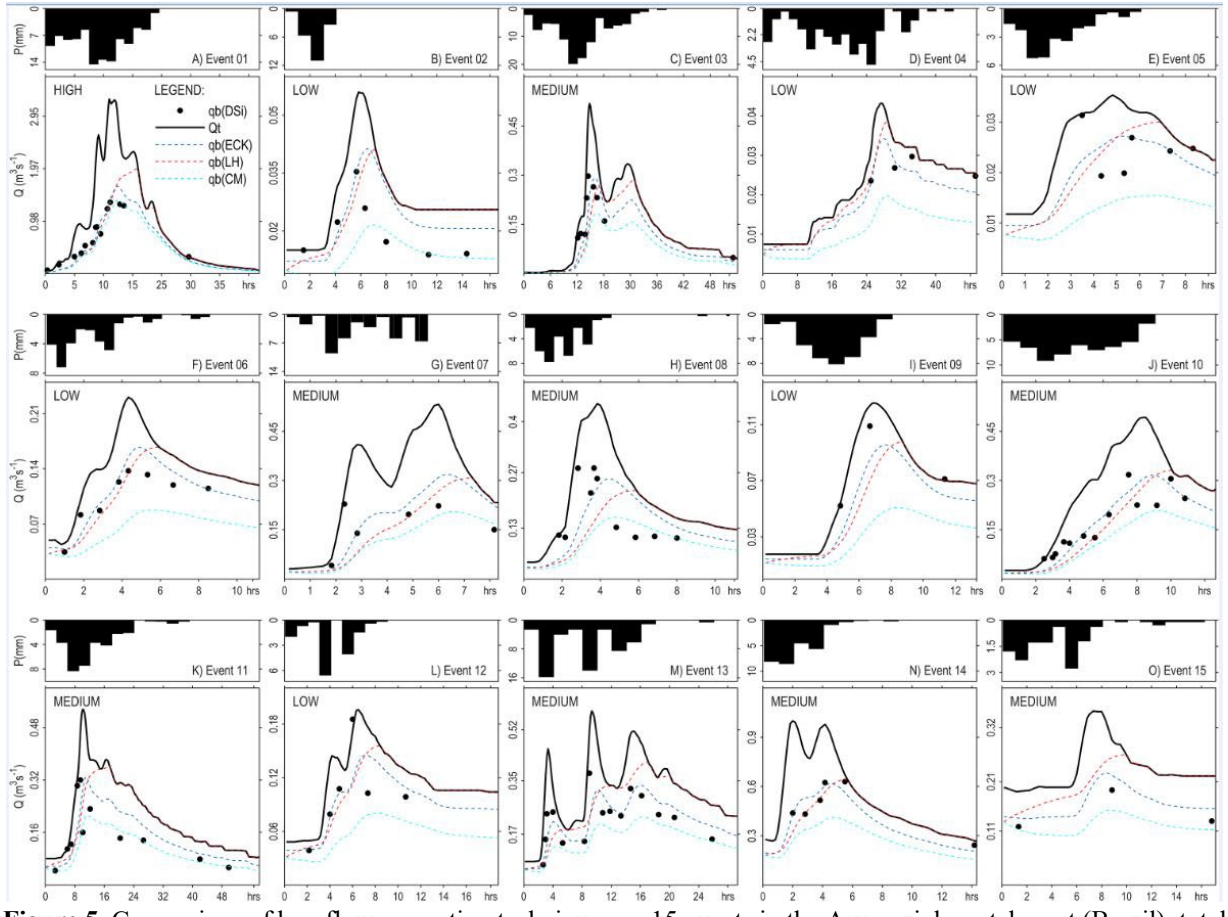

Figure 5. Comparison of baseflow separation techniques on 15 events in the Arvorezinha catchment (Brazil): total streamflow (*Qt*) as solid black curves; silica-derived baseflow (*qb(DSi)*) as black dots; Eckhardt's filter baseflow (*qb(ECK)*)

https://doi.org/10.5194/egusphere-2025-244
Preprint. Discussion started: 26 March 2025

in blue dotted lines; LH filter baseflow (*qb(LH)*) in red dotted lines; and CM filter baseflow (*qb(CM)*) in cyan dotted lines. Note: Eckhardt's and LH filters used varying parameters as a function of event magnitude (low, medium or high).

Visual inspection of **Fig. 5** (event-based calibration results) and **Fig. 2** (general calibration results) does not allow for an accurate determination of the changes brought about by the event-based calibration, as similar observations can be noted for both calibration processes. Eckhardt's filter and CM filter yielded more plausible baseflow hydrographs in terms of shape (both follow the smoothness of the streamflow hydrographs and present a reasonably delayed peak in comparison to the peak observed on the streamflow hydrograph). In terms of volume, the Eckhardt's filter shows higher volumes than the CM model. The LH model resulted in overall higher baseflow volumes than the other two models. The baseflow estimated by the LH model increases gradually and achieves its maximum rate near the end of the direct runoff hydrograph, presenting a higher delay in baseflow peak, as compared to the other two methods. The event-based calibration led to a reduction of the delay between baseflow and streamflow peaks. For the Eckhardt's filter, the average event delay was calculated as 1.5 hours using the general calibration, which reduced to 1.3 hours with the event-based calibration. For the LH filter, the average event delay reduced from 4.4 hours (general calibration) to 3.4 hours (event-based calibration).

Table 7 shows the performance indicators *PBias, NSE, KGE,* and *NRMSD* computed for the Eckhardt's and LH filters after the event-based calibration. These metrics were calculated comparing modelled baseflows with baseflow values derived from DSi data. The asterisks (*) show the level of improvement in the performance indicators, compared to the general calibration. The event-based calibration has significantly improved the metrics for both models.

Table 7. Error metrics comparison for observed (DSi-derived) *versus* modeled baseflows considering 15 events and two separation methods adopting the following parameters: Eckhardt's filter (a = 0.952, $BFI_{max}^{(low)}$ = 0.809, $BFI_{max}^{(medium)}$ = 0.701, $BFI_{max}^{(high)}$ = 0.576); LH filter ($\beta^{(low)}$ = 0.921, $\beta^{(medium)}$ = 0.957, $\beta^{(high)}$ = 0.970). The criteria for acceptable model performance were defined as *NSE* > 0.5, *KGE* > -0.41, *NRMSD* < 10% and *PBias* < +/- 25%

Filter	*PBias* (%)	*NSE*	*KGE*	*NRMSD* (%)
Eckhardt	< 0.50	0.92***	0.91****	5.4**
LH	< 1.20	0.84**	0.85***	7.8*

Improvement in relation to the general calibration: *5-20%; **20-35%; ***35-50%; ****>50%. The absence of a (*) indicates no significant improvement.

Following the event-based calibration, the *BF* ratios were computed as 65% for the Eckhardt's model and 76% for the LH model, representing a slight change from the general calibration outcomes of 64% for Eckhardt's and 75% for LH. The *BF* ratio from the Eckhardt's filter remains the most accurate, aligning more closely with the DSi-derived *BF* ratio of 66%. Correspondingly, the coefficient of variation (CV) for the Eckhardt's filter showed an increase from the general calibration, a result anticipated due to the application of varying BFI_{max} values, which naturally led to greater variability across the events. The *BF* ratios computed after the event-based calibration alongside reference values are summarized in **Table 8**.

https://doi.org/10.5194/egusphere-2025-244
Preprint. Discussion started: 26 March 2025

Table 8. Comparative analysis of average *BF* ratios for the Arvorezinha Catchment (1.2 km²) in Southern Brazil across 15 rainfall-runoff events using various baseflow separation methods and an event-based calibration approach, alongside literature reference values.

Separation Method	***BF* ratio (average of 15 rainfall-runoff events)**	**Reference values of *BF* ratios for catchments similar to the study area or catchments located in the South of Brazil**
Mass balance (DSi-derived baseflows)	66% CV = 0.19	• 60-72% for rhyodacite catchments in Australia (Lacey & Grayson, 1998) • 67-91% for basalt catchments in Australia (Lacey & Grayson, 1998) • 50-70% for basalt catchments in the same hydrographic region in Brazil (Chagas et al., 2020) • 54-65% for catchments overlying igneous aquifers in southeastern Brazil (Santarosa et al., 2023) • 60-64% for small rural catchments overlying igneous aquifers in Kenya (Mugo & Sharma, 1999) • 61% for six small rural catchments over granite and gneiss in Southeastern Brazil (Costa & Bacellar, 2009) • 63% for catchments in C_f climate regions (Beck et al., 2013) • 60% for catchments in the south of Brazil (Tan et al., 2020) • 65% for catchments underlain with basalt and granite in Tanzania (Mwakalila et al., 2002) • 50-70% is the predominant *BF* ratio in an analysis of 1815 undisturbed catchments in the USA. It occurs in 50% of the catchments (Xie et al., 2020)
Eckhardt's Filter (general calibration) (a = 0.952; BFI_{max} = 0.653)	64% CV = 0.04	
Eckhardt's Filter (event-based calibration) (a = 0.952; $BFI_{max}^{(low)}$ = 0.809, $BFI_{max}^{(medium)}$ = 0.701, $BFI_{max}^{(high)}$ = 0.576)	65% CV = 0.09	
LH Filter (calibrated) (β= 0.965)	75% CV = 0.15	
LH Filter (event-based calibration) ($\beta^{(low)}$ = 0.921, $\beta^{(medium)}$ = 0.957, $\beta^{(high)}$ = 0.970)	76% CV = 0.14	
CM Filter (a = 0.952)	48% CV = 0.06	

510

Figure 6 illustrates the relationship between modeled and observed baseflows for the Eckhardt and LH filters, comparing results from both general and event-based calibration methods. This comparison highlights the improvement in model performance following the event-based calibration. Specifically, this approach has led to improved predictions of the data extremes, including both low and high flows, which were not accurately predicted with the general calibration process.

https://doi.org/10.5194/egusphere-2025-244
Preprint. Discussion started: 26 March 2025

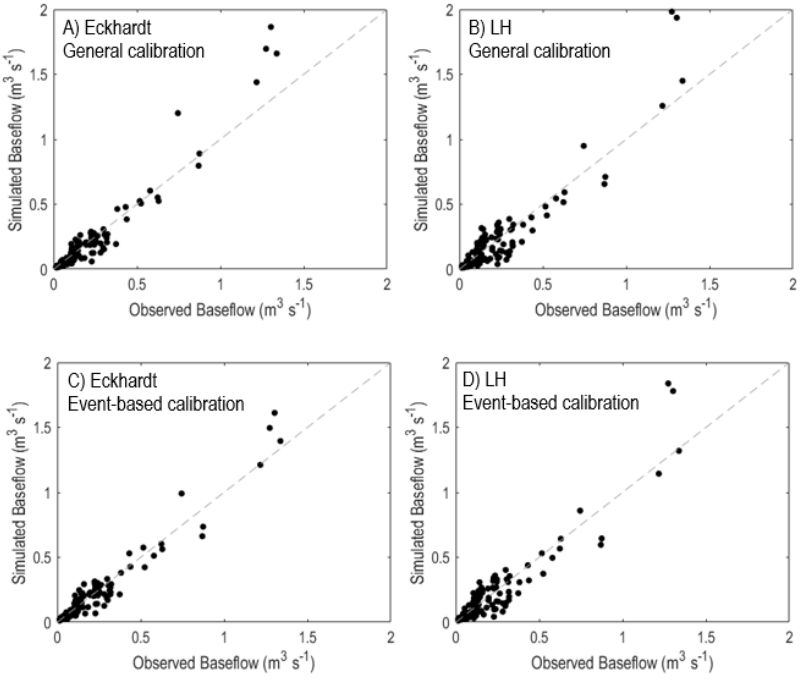

Figure 6: Scatter plot comparing modeled baseflow values against observed values derived from DSi, with the grey dashed line representing the 1:1 line. Eckhardt – General calibration (A), LH – General Calibration (B), Eckhardt – Event-based calibration (C), LH – Event-based Calibration (D). The plots show the higher performance of the models under event-based calibration, particularly with a better prediction oh high flows in comparison to the general calibration approach.

An analysis of individual events, as detailed in **Tables 9** and **10**, indicates that the event-based calibration led to improvements in performance metrics for both the LH and Eckhardt's filters across most events. The data highlight that, for the Eckhardt's filter, the event calibration approach enhanced the *PBias* indicator in 12 events, *NSE* in 10 events, and *NRMSD* in nine events. Regarding the LH filter, there were enhancements observed in the *PBias* and *NSE* metrics for nine events, and in the *NRMSD* for seven events. These enhancements emphasize the efficacy of the calibrated models in accurately predicting baseflows for almost all the events, illustrating that a calibration tailored to specific event magnitudes can result in more accurate modeling outcomes than a generic calibration approach.

https://doi.org/10.5194/egusphere-2025-244
Preprint. Discussion started: 26 March 2025

Table 9. Error metrics comparison for observed versus simulated baseflows across 15 events, utilizing the event-based calibration of the **Eckhardt's filter** (a = 0.952, $BFI_{max}^{(low)}$ = 0.809, $BFI_{max}^{(medium)}$ = 0.701, $BFI_{max}^{(high)}$ = 0.576). The criteria for acceptable model performance were defined as *NSE* > 0.50, *KGE* > -0.41, *NRMSD* < 10% and *PBias* < +/- 25%

Event - Magnitude	Q_{max} (l.s^{-1})	DSi samples	*PBias* (%)	*NSE*	*KGE*	*NRMSD* (%)	*BF ratio*
1 – High	3277.6	14	0.1****	0.88****	0.78****	11.7***	0.56
2 – Low	56.0	7	25.7$^{\#\#\#\#}$	-0.44 $^{\#\#\#\#}$	0.49	41.1$^{\#\#}$	0.79
3 – Medium	518.4	9	-12.6*	0.45**	0.73*	23.5*	0.69
4 – Low	43.2	4	-6.5****	-0.58****	0.52	47.7****	0.79
5 – Low	35.3	6	0.7****	-0.77***	-0.56*	45.4**	0.78
6 – Low	230.8	8	6.6****	0.72***	0.68 $^{\#\#\#}$	16.5**	0.78
7 – Medium	532.4	6	2.3****	-0.63 $^{\#}$	0.31 $^{\#}$	43.6	0.62
8 – Medium	445.3	10	-3.9****	-0.12*	0.36*	44.5	0.67
9 – Low	125.1	3	-24.5***	0.30****	0.75****	34.7***	0.78
10 – Medium	493.0	13	-0.4****	0.76	0.78 $^{\#\#}$	16.4	0.65
11 – Medium	535.1	11	4.7 $^{\#}$	0.31	0.65*	26.7	0.69
12 – Low	195.8	6	-3.9****	0.43***	0.59**	22.6**	0.79
13 – Medium	582.7	15	-2.2****	0.43*	0.70*	18.7*	0.69
14 – Medium	998.0	6	0.7****	0.81**	0.90**	14.7*	0.68
15 - Medium	353.2	3	16.5 $^{\#\#\#\#}$	0.42 $^{\#\#\#\#}$	0.78 $^{\#\#\#\#}$	33.4$^{\#\#\#\#}$	0.68
All events combined		121	< 0.50	0.92***	0.91****	5.4**	0.65

Changes relative to the general calibration: *5-20%; **20-35%; ***35-50%; ****>50% improvement. $^{\#}$ 5-20%; $^{\#\#}$20-35%; $^{\#\#\#}$35-50%; $^{\#\#\#\#}$>50% worsening. The absence of (*) or ($^{\#}$) indicates no significant change.

Table 10. Error metrics comparison for observed versus simulated baseflows across 15 events, utilizing the event-based calibration of the **LH filter** ($\beta^{(low)}$ = 0.921, $\beta^{(medium)}$ = 0.957, $\beta^{(high)}$ = 0.970). The criteria for acceptable model performance were defined as *NSE* > 0.50, *KGE* > -0.41, *NRMSD* < 10% and *PBias* < +/- 25%

Event - Magnitude	Q_{max} (l.s^{-1})	DSi samples	*PBias* (%)	*NSE*	*KGE*	*NRMSD* (%)	*BF ratio*
1 – High	3277.6	14	-0.3***	0.70**	0.64**	18.3*	0.67
2 – Low	56.0	7	26.9 $^{\#\#\#\#}$	-0.87	0.35***	46.8	0.86
3 – Medium	518.4	9	-27.6**	-0.20*	0.52*	34.7*	0.80
4 – Low	43.2	4	10.0 $^{\#\#\#\#}$	-1.38	0.26***	58.5	0.94
5 – Low	35.3	6	4.4****	-1.40**	-0.48 $^{\#}$	52.9*	0.81
6 – Low	230.8	8	4.3 $^{\#}$	0.50***	0.57 $^{\#\#}$	22.2**	0.82
7 – Medium	532.4	6	-14.4**	-0.93	0.27	47.4	0.54
8 – Medium	445.3	10	-18.5**	-1.01*	-0.14*	59.6	0.67
9 – Low	125.1	3	-28.5**	-0.32****	0.61****	47.8***	0.80
10 – Medium	493.0	13	-6.7****	0.63*	0.63 $^{\#}$	20.3	0.64
11 – Medium	535.1	11	14.8 $^{\#\#\#\#}$	-0.17	0.43*	34.9	0.90
12 – Low	195.8	6	-4.3****	0.23***	0.53**	26.2**	0.88
13 – Medium	582.7	15	12.3 $^{\#\#\#\#}$	-0.53	0.39	30.7	0.84

https://doi.org/10.5194/egusphere-2025-244
Preprint. Discussion started: 26 March 2025

14 – Medium	998.0	6	-3.9****	0.83****	0.92****	14.1**	0.77
15 - Medium	353.2	3	41.9 #	-3.20 #	0.37 #	90.1 #	0.87
All events combined		121	< 1.20	0.84**	0.85***	7.8*	0.76

Changes relative to the general calibration: *5-20%; **20-35%; ***35-50%; ****>50% improvement. # 5-20%; ##20-35%; ###35-50%; ### >50% worsening. The absence of (*) or (#) indicates no significant change.

4. Considerations for using the DSi mass-balance method to calibrate RDF filters

The calibration of BFI_{max} and *Beta* parameters using the DSi mass-balance approach requires careful attention due to fundamental differences in how flow components are distinguished. RDFs primarily separate baseflow and quickflow based on flow velocity characteristics (Helfer et al., 2024), whereas the mass-balance technique relies on variations in DSi concentrations. This contrast is especially important in larger catchments, where transient water contributions, such as the mobilization of older stored water and return flow processes, can substantially impact hydrograph responses (Cartwright et al., 2018; Yang et al., 2021).

RDF filters differentiate baseflow as slow-moving components like groundwater and bank storage return flow, while identifying quickflow as rapid-response flows, including surface runoff, soil interflow, and direct precipitation. Conversely, the DSi mass-balance method classifies flow components based on DSi concentrations, designating high-DSi components (groundwater and old-water flushing) as baseflow and low-DSi components (surface runoff, return flow, and direct precipitation) as quickflow.

During storm events, these differences become particularly pronounced. Old-water flushing introduces a rapid increase in DSi concentrations early in the hydrograph, reflecting the displacement of solute-rich water stored in the soil matrix. While the mass-balance method captures this as baseflow, RDF filters, designed to represent the gradual response of slow groundwater movement, assign such flows to quickflow. Similarly, bank storage return flow, characterized by dilution effects, is considered baseflow in RDF filters but quickflow in the mass-balance method. These contrasting classifications can result in misaligned peak timings and differing baseflow dynamics, particularly in short-term hydrographs.

In the Arvorezinha catchment, where transient water effects such as old-water flushing and return flow are minimal due to its shallow, clayey soils, the DSi mass-balance method and RDF filters can be reasonably aligned for calibration. However, during some events, discrepancies were observed. For example, events 2, 9, and 9 showed earlier baseflow peaks in the mass-balance method, likely caused by old-water flushing. This initial peak was subsequently reduced as event groundwater and return flows, with lower DSi concentrations, diluted the streamflow.

Although the mass-balance method may not be ideal for short-term baseflow separation (hourly or daily) due to transient water effects, it is still well-suited for long-term applications. Over extended periods, the calibrated filters, particularly the Eckhardt's filter, ensure cumulative baseflow estimates are consistent with those of the DSi method. To enhance the reliability of such calibrations, validating results against reported *BFI* values from the literature is strongly recommended (Helfer et al., 2024).

https://doi.org/10.5194/egusphere-2025-244
Preprint. Discussion started: 26 March 2025

Ultimately, the differences between the two methods highlight the need for a nuanced application of the mass-balance method in calibrating RDF filters. Future studies could focus on combining both approaches to create multi-component streamflow separation methods or assess the impact of transient water sources, providing deeper insights into hydrological processes and flow dynamics.

5. Conclusions and final considerations

This study covered a detailed examination of baseflow separation techniques within a small rural catchment, applying both general and event-based calibration strategies to optimize the parameters of Eckhardt's, Lyne and Hollick (LH), and Chapman and Maxwell (CM) filters. The initial objective of calibrating BFI_{max} (Eckhardt's) and *Beta* (LH) parameters to minimize differences between modeled and tracer-based baseflow values was successfully achieved, with both filters demonstrating improved accuracy over the CM method.

The CM model, reliant solely on streamflow and the recession constant, lacked the flexibility for fine-tuning, restricting its accuracy in volume and peak magnitude estimation, with a notable average underestimation of baseflow quantities by 28%. On the other hand, the flexibility of the adjustable parameters in the Eckhardt's and LH models enabled a more precise representation of baseflow hydrographs after calibration. Optimal calibration yielded BFI_{max} and *Beta* values of 0.653 and 0.965, respectively, with the Eckhardt's filter slightly outperforming the LH model across several metrics, including the Nash-Sutcliffe efficiency, Kling-Gupta efficiency, and normalized root mean square deviation. This superiority extended to capturing peak timings and the shape of baseflow hydrographs, corroborated by stable and credible baseflow index values aligned with existing literature for comparable catchments.

The introduction of an event-based calibration approach in this study marked a significant advancement in the field, demonstrating that baseflow separation accuracy could be enhanced by adjusting the BFI_{max} and *Beta* parameters according to the magnitude of rainfall-runoff events. This approach yielded more precise baseflow estimations, as evidenced by improved performance indicators and a closer agreement with observed data. The findings thus revealed that the parameters BFI_{max} and *Beta* are not static but vary with event characteristics, highlighting the importance of the development of flexible calibration approaches for the Eckhardt's and LH filters. Recommended BFI_{max} values for varying event magnitudes ranged from 0.809 for low to 0.576 for high-magnitude events, while optimal *Beta* values ranged from 0.921 for low to 0.970 for high-magnitude events.

The superior performance of the Eckhardt's filter, particularly under the event-based calibration, indicates that this filter offers the most robust method for baseflow separation in small rural catchments. In scenarios where tracer data is available for calibration, the Eckhardt's filter is the preferred choice, with the potential for enhanced accuracy through event magnitude calibration. In the absence of such data, practitioners should attempt to identify a catchment-specific BFI_{max} value, informed by a review of the relevant literature. In catchments similar to the one studied – marked by their small area, pronounced slopes,

https://doi.org/10.5194/egusphere-2025-244
Preprint. Discussion started: 26 March 2025

rapid baseflow recession, and porous soils over fractured basaltic bedrock – a BFI_{max} value of 0.653 is proposed as an initial reference point. Relying on a standard value of 0.25 is discouraged, as it could substantially underestimate baseflow quantities. Additionally, the results of event-specific calibration demonstrated that a 'one-size-fits-all' approach to BFI_{max} or *Beta* may not always yield optimal results, potentially leading to inaccuracies in high- and low-flow conditions.

Future research should focus on expanding the calibration of RDFs to a broader range of catchments with varying hydrological characteristics, and including a wider range of rainfall-runoff events with various magnitudes. Additionally, exploring the potential for further refinement of the CM model, despite its lack of adjustable parameters, could provide a more comprehensive understanding of its application scope. As the body of research in this area grows, it will become possible to formulate universal protocols for the effective use and optimization of RDFs.

6. Acknowledgements

Funding for this research was partially provided by the *Coordenação de Aperfeiçoamento de Pessoal de Nível Superior - Brazil (CAPES)* under Finance Code 001. We express our gratitude for the *Young Talent Grant* (reference number 88887.893273/2023-00), jointly supported by *CAPES* and the *Federal University of Santa Maria (UFSM)*, awarded to Dr. Fernanda Helfer. Additional appreciation goes to Brazilian agencies like *FAPERGS* and *CNPq,* whose financial support has been vital for sustaining ongoing research efforts at the Arvorezinha catchment. We also wish to recognize *Griffith University* (Australia) for enabling Dr. Fernanda Helfer's involvement in this Brazilian project through the *Griffith Academic Studies Program 2023-2024*. Finally, while AI tools assisted with linguistic polishing, we confirm that all concepts, text, and scientific contributions in this work are entirely human-generated.

7. Data Availability

The data that support the findings of this study are available from the corresponding author upon request.

8. Author contribution

FH: Conceptualization, Methodology, Software, Validation, Formal Analysis, Investigation, Resources, Data Curation, Writing – Original Draft, Writing – Review & Editing, Visualization, Project Administration, Funding Acquisition. **FB:** Conceptualization, Methodology, Software, Validation, Formal Analysis, Investigation, Data Curation, Visualization, Funding Acquisition. **CB:** Conceptualization, Methodology, Validation, Investigation, Resources, Data Curation. **DA**: Conceptualization, Methodology, Validation, Investigation, Resources, Supervision, Project Administration, Funding

https://doi.org/10.5194/egusphere-2025-244
Preprint. Discussion started: 26 March 2025

Acquisition. **JM:** Investigation, Resources, Supervision, Funding Acquisition. **RT:** Conceptualization, Methodology, Investigation, Resources, Project Administration. **NS**: Formal Analysis, Investigation, Visualization.

9. Competing interests

The authors declare that they have no known competing financial interests or personal relationships that could have appeared to influence the work reported in this paper.

10. References

Ahiablame, L., Chaubey, I., Engel, B., Cherkauer, K., and Merwade, V.: Estimation of annual baseflow at ungauged sites in Indiana, USA, J. Hydrol., 476, 13–27, https://doi.org/10.1016/j.jhydrol.2012.10.002, 2013.

Amorim, J. D., Viola, M. R., Junqueira, R., de Mello, C. R., Bento, N. L., and Avanzi, J. C.: Quantifying the climate change-driven impacts on the hydrology of a data-scarce watershed located in the Brazilian Tropical Savanna, Hydrol. Process., 36, e14638, https://doi.org/10.1002/hyp.14638, 2022.

Apurv, T. and Cai, X. M.: Impact of droughts on water supply in US watersheds: The role of renewable surface and groundwater resources, Earth's Future, 8, e2020EF001648, https://doi.org/10.1029/2020EF001648, 2020.

Arnold, J. G. and Allen, P. M.: Automated methods for estimating baseflow and groundwater recharge from streamflow records, J. Am. Water Resour. Assoc., 35, 411–424, https://doi.org/10.1111/j.1752-1688.1999.tb03599.x, 1999.

Arnold, J. G., Allen, P. M., Muttiah, R., and Bernhardt, G.: Automated base-flow separation and recession analysis techniques, Ground Water, 33, 1010–1018, https://doi.org/10.1111/j.1745-6584.1995.tb00046.x, 1995.

Asano, Y., Uchida, T., and Ohte, N.: Hydrologic and geochemical influences on the dissolved silica concentration in natural water in a steep headwater catchment, Geochim. Cosmochim. Ac., 67, 1973–1989, https://doi.org/10.1016/S0016-7037(02)01342-X, 2003.

Basso, R. E., Allasia, D. G., and Tassi, R.: Vazão de projeto na microdrenagem em locais sem dados de precipitação: estudo para o Rio Grande do Sul, Ambiente Construído, 19, https://doi.org/10.1590/s1678-86212019000300335, 2019.

Beatty, S. J., Morgan, D. L., McAleer, F. J., and Ramsay, A. R.: Groundwater contribution to baseflow maintains habitat connectivity for (Teleostei: Plotosidae) in a south-western Australian river, Ecol. Freshw. Fish, 19, 595–608, https://doi.org/10.1111/j.1600-0633.2010.00440.x, 2010.

Beck, H. E., van Dijk, A. I. J. M., Miralles, D. G., de Jeu, R. A. M., Bruijnzeel, L. A., McVicar, T. R., and Schellekens, J.: Global patterns in baseflow index and recession based on streamflow observations from 3394 catchments, Water Resour. Res., 49, 7843–7863, https://doi.org/10.1002/2013WR013918, 2013.

Beighley, R. E., Dunne, T., and Melack, J. M.: Understanding and modeling basin hydrology: interpreting the hydrogeological signature. Hydrol. Proc., 19, 1333-1353. https://doi.org/10.1002/hyp.5567, 2005.

https://doi.org/10.5194/egusphere-2025-244
Preprint. Discussion started: 26 March 2025

Bell, F. C.: Generalized rainfall-duration-frequency relationships, J. Hydraul. Div., 95, 311–328, https://doi.org/10.1061/JYCEAJ.0001942, 1969.

Bloomfield, J. P., Allen, D. J., and Griffiths, K. J.: Examining geological controls on baseflow index (BFI) using regression analysis: An illustration from the Thames Basin, UK, J. Hydrol., 373, 164–176, https://doi.org/10.1016/j.jhydrol.2009.04.025, 2009.

Buttle, J. M. and Peters, D. L.: Inferring hydrological processes in a temperate basin using isotopic and geochemical hydrograph separation: A re-evaluation, Hydrol. Process., 11, 557–573, https://doi.org/10.1002/(Sici)1099-1085(199705)11:6<557::Aid-Hyp477>3.0.Co;2-Y, 1997.

Cartwright, I., Atkinson, A.P., Gilfedder, B.S., Hofmann, H., Cendón, D.I., and Morgenstern, U. Using geochemistry to understand water sources and transit times in headwater streams of a temperate rainforest, App. Geochem., 99, 1-12. https://doi.org/10.1016/j.apgeochem.2018.10.018, 2018.

Chapman, T. G. and Maxwell, A. I.: Baseflow separation – comparison of numerical methods with tracer experiments, in: Hydrology and Water Resources Symposium 1996: Water and the Environment, Barton, Australia, 539–546, 1996.

Cheng, S., Tong, X., and Illman, W. A.: Evaluation of baseflow separation methods with real and synthetic streamflow data from a watershed, J. Hydrol., 613, 128279, https://doi.org/10.1016/j.jhydrol.2022.128279, 2022.

USGS: Operating instructions for US DH-48 suspended-sediment hand sample, Report produced for the Federal Interagency Sedimentation Project, available at: https://water.usgs.gov/fisp/docs/Report_J.pdf (last access: January 2025), 1965.

Collischonn, W. and Fan, F. M.: Defining parameters for Eckhardt's digital baseflow filter, Hydrol. Process., 27, 2614–2622, https://doi.org/10.1002/hyp.9391, 2013.

Cook, P. G.: The role of tracers in hydrogeology, Groundwater, 53, 1–2, https://doi.org/10.1111/gwat.12327, 2015.

Costa, F. M. and Bacellar, L. A. P.: The hydrogeologic potential conditioning factors of hydrographic catchments of Upper Velhas River Basin, Southeastern Brazil, Environ. Earth Sci., 59, 87–97, https://doi.org/10.1007/s12665-009-0007-7, 2009.

CSIRO and SKM: Baseflow assessment for the Murray-Darling Basin, CSIRO: Water for a Healthy Country National Research Flagship, 78 pp., 2010.

de Barros, C. A. P.: Dinâmica dos escoamentos na modelagem da produção de sedimentos em uma pequena bacia rural, PhD thesis, Centro de Ciências Rurais, UFSM, Santa Maria, Brazil, 195 pp., 2016.

de Barros, C. A. P., Govers, G., Minella, J. P. G., and Ramon, R.: How water flow components affect sediment dynamics modeling in a Brazilian catchment, J. Hydrol., 597, 126111, https://doi.org/10.1016/j.jhydrol.2021.126111, 2021.

de Barros, C. A. P., Minella, J. P. G., Dalbianco, L., and Ramon, R.: Description of hydrological and erosion processes determined by applying the LISEM model in a rural catchment in southern Brazil, J. Soils Sediments, 14, 1298–1310, https://doi.org/10.1007/s11368-014-0903-7, 2014.

Eckhardt, K.: How to construct recursive digital filters for baseflow separation, Hydrol. Process., 19, 507–515, https://doi.org/10.1002/hyp.5675, 2005.

https://doi.org/10.5194/egusphere-2025-244
Preprint. Discussion started: 26 March 2025

Eckhardt, K.: A comparison of baseflow indices, which were calculated with seven different baseflow separation methods, J. Hydrol., 352, 168–173, https://doi.org/10.1016/j.jhydrol.2008.01.005, 2008.

Eckhardt, K.: Technical Note: Analytical sensitivity analysis of a two-parameter recursive digital baseflow separation filter, Hydrol. Earth Syst. Sci., 16, 451–455, https://doi.org/10.5194/hess-16-451-2012, 2012.

Fetter, C. W.: Applied Hydrogeology, 4th Edn., Prentice Hall, 624 pp., 2001.

Furey, P. R. and Gupta, V. K.: A physically based filter for separating baseflow from streamflow time series, Water Resour. Res., 37, 2709–2722, https://doi.org/10.1029/2001wr000243, 2001.

Glas, R., Hecht, J., Simonson, A., Gazoorian, C., and Schubert, C.: Adjusting design floods for urbanization across groundwater-dominated watersheds of Long Island, NY, J. Hydrol., 618, 129194, https://doi.org/10.1016/j.jhydrol.2023.129194, 2023.

Gómez, D., Wendland, E., and Melo, D. D. D.: Empirical rainfall-based model for defining baseflow and dynamical water use rights, River Res. Appl., 36, 189–198, https://doi.org/10.1002/rra.3565, 2020.

Gonzales, A. L., Nonner, J., Heijkers, J., and Uhlenbrook, S.: Comparison of different baseflow separation methods in a lowland catchment, Hydrol. Earth Syst. Sci., 13, 2055–2068, https://doi.org/10.5194/hess-13-2055-2009, 2009.

Gupta, H. V., Kling, H., Yilmaz, K. K., and Martinez, G. F.: Decomposition of the mean squared error and NSE performance criteria: Implications for improving hydrological modelling, J. Hydrol., 377, 80–91, https://doi.org/10.1016/j.jhydrol.2009.08.003, 2009.

Gupta, H. V., Sorooshian, S., and Yapo, P. O.: Status of automatic calibration for hydrologic models: Comparison with multilevel expert calibration, J. Hydrol. Eng., 4, 135–143, https://doi.org/10.1061/(ASCE)1084-0699(1999)4:2(135), 1999.

Haberlandt, U., Klöcking, B., Krysanova, V., and Becker, A.: Regionalisation of the base flow index from dynamically simulated flow components – A case study in the Elbe River Basin, J. Hydrol., 248, 35–53, https://doi.org/10.1016/S0022-1694(01)00391-2, 2001.

Helfer, F., Bernardi, F. K., de Barros, C. A. P., Piccilli, D. G. A., Minella, J. P. G., Tassi, R., and Schlesner, A. A.: Calibrated Eckhardt's filter versus alternative baseflow separation methods: A silica-based approach in a Brazilian catchment, J. Hydrol., 644, 132073, https://doi.org/10.1016/j.jhydrol.2024.132073, 2024.

Hendershot, W. H., Savoie, S., and Courchesne, F.: Simulation of stream-water chemistry with soil solution and groundwater-flow contributions, J. Hydrol., 136, 237–252, https://doi.org/10.1016/0022-1694(92)90013-L, 1992.

Hinton, M. J., Schiff, S. L., and English, M. C.: Examining the contributions of glacial till water to storm runoff using 2-component and 3-component hydrograph separations. Water Resour. Res., 30, 983-993. https://doi.org/10.1029/93wr03246, 1994.

Hugenschmidt, C., Ingwersen, J., Sangchan, W., Sukvanachaikul, Y., Duffner, A., Uhlenbrook, S., and Streck, T.: A three-component hydrograph separation based on geochemical tracers in a tropical mountainous headwater catchment in northern Thailand. Hydrol. Earth Syst. Sci, 18, 525-537. https://doi.org/10.5194/hess-18-525-2014, 2014.

https://doi.org/10.5194/egusphere-2025-244
Preprint. Discussion started: 26 March 2025

Indarto, Novita, E., and Wahyuningsih, S.: Preliminary study on baseflow separation at watersheds in East Java regions, Agric. Agric. Sci. Procedia, 9, 538–550, https://doi.org/10.1016/j.aaspro.2016.02.174, 2016.

Jain, M. K.: Recession of discharge, in: Encyclopedia of Snow, Ice and Glaciers, edited by: Singh, V. P., Singh, P., and Haritashya, U. K., Springer Netherlands, Dordrecht, 922–924, https://doi.org/10.1007/978-90-481-2642-2_437, 2011.

Kang, T., Lee, S., Lee, N., and Jin, Y.: Baseflow separation using the digital filter method: Review and sensitivity analysis, Water, 14, 30485, https://doi.org/10.3390/w14030485, 2022.

Khan, A., Umar, R., and Khan, H. H.: Significance of silica in identifying the processes affecting groundwater chemistry in parts of Kali watershed, Central Ganga Plain, India. Appl. Water Sci., 5, 65-72, https://doi.org/10.1007/s13201-014-0164-z, 2015.

Kennedy, V. C.: Silica variation in stream water with time and discharge, Adv. Chem. Ser., 106, 94–130, https://doi.org/10.1021/ba-1971-0106.ch004, 1971.

Knoben, W. J. M., Freer, J. E., and Woods, R. A.: Technical note: Inherent benchmark or not? Comparing Nash-Sutcliffe and Kling-Gupta efficiency scores, Hydrol. Earth Syst. Sci., 23, 4323-4331, https://doi.org/10.5194/hess-23-4323-2019, 2019.

Kouanda, B., Coulibaly, P., Niang, D., Fowe, T., Karambiri, H., and Paturel, J. E.: Analysis of the performance of base flow separation methods using chemistry and statistics in Sudano-Sahelian watershed, Burkina Faso, Hydrol. Curr. Res., 9, 1000300, https://doi.org/10.4172/2157-7587.1000300, 2018.

Lacey, G. C. and Grayson, R. B.: Relating baseflow to catchment properties in south-eastern Australia, J. Hydrol., 204, 231–250, https://doi.org/10.1016/S0022-1694(97)00124-8, 1998.

Ladson, A. R., Brown, R., Neal, B., and Nathan, R.: A standard approach to baseflow separation using the Lyne and Hollick filter, Australas. J. Water Resour., 17, 25–34, https://doi.org/10.7158/13241583.2013.11465417, 2013.

Latuamury, B., Osok, R. M., Puturuhu, F., and Imlabla, W. N.: Baseflow separation using graphic method of recursive digital filter on Wae Batu Gajah Watershed, Ambon City, Maluku, IOP Conf. Ser.: Earth Environ. Sci., 989, 012028, https://doi.org/10.1088/1755-1315/989/1/012028, 2022.

Laudon, H. and Slaymaker, O.: Hydrograph separation using stable isotopes, silica and electrical conductivity: An alpine example, J. Hydrol., 201, 82–101, https://doi.org/10.1016/S0022-1694(97)00030-9, 1997.

Lei, Y. N., Zhang, X. P., Ma, Q., Sun, Y. P., Zhang, J. J., Fu, Y. L., and Xu, J. P.: Responses of baseflow in Kuye catchment to the LUCC on the Loess Plateau of China, in: 19th International Congress on Modelling and Simulation (MODSIM2011), Perth, Australia, 3594–3600, https://doi.org/10.36334/modsim.2011.i6.lei, 2011.

Li, L., Maier, H. R., Lambert, M. P., Simmons, C. T., and Partington, D.: Framework for assessing and improving the performance of recursive digital filters for baseflow estimation with application to the Lyne and Hollick filter, Environ. Model. Softw., 41, 163–175, https://doi.org/10.1016/j.envsoft.2012.11.009, 2013.

https://doi.org/10.5194/egusphere-2025-244
Preprint. Discussion started: 26 March 2025

Longobardi, A. and Villani, P.: Baseflow index characterization in typical temperate to dry climates: Conceptual analysis and simulation experiment to assess the relative role of climate forcing features and catchment geological settings, Hydrol. Res., 54, 136–148, https://doi.org/10.2166/nh.2023.026, 2023.

Lyne, V. and Hollick, M.: Stochastic time-variable rainfall-runoff modelling, in: Institute of Engineers Australia National Conference, Perth, Australia, 379–387, available at: https://www.researchgate.net/publication/272491803, 1979.

Marçais, J., Gauvain, A., Labasque, T., Abbott, B. W., Pinay, G., Aquilina, L., Chabaux, F., Viville, D., and de Dreuzy, J. R.: Dating groundwater with dissolved silica and CFC concentrations in crystalline aquifers. Sci. Total Environ., 636, 260-272. https://doi.org/10.1016/j.scitotenv.2018.04.196, 2018.

Mau, D. P. and Winter, T. C.: Estimating ground-water recharge from streamflow hydrographs for a small mountain watershed in a temperate humid climate, New Hampshire, USA, Groundwater, 35, 291–304, https://doi.org/10.1111/j.1745-6584.1997.tb00086.x, 1997.

Mazvimavi, D., Meijerink, A. M. J., and Stein, A.: Prediction of base flows from basin characteristics: A case study from Zimbabwe, Hydrol. Sci. J., 49, 703–715, https://doi.org/10.1623/hysj.49.4.703.54428, 2004.

Mehaiguene, M., Meddi, M., Longobardi, A., and Toumi, S.: Low flows quantification and regionalization in North West Algeria, J. Arid Environ., 87, 67–76, https://doi.org/10.1016/j.jaridenv.2012.07.014, 2012.

Merten, G. H. and Minella, J. P. G.: Impact on sediment yield due to intensification of tobacco production in a catchment in southern Brazil, Sediment Budgets 2, 292, 239–244, https://doi.org/10.1590/S0103-84782006000200050, 2005.

Miller, M. P., Buto, S. G., Susong, D. D., and Rumsey, C. A.: The importance of base flow in sustaining surface water flow in the Upper Colorado River Basin, Water Resour. Res., 52, 3547–3562, https://doi.org/10.1002/2015wr017963, 2016.

Minea, I.: Streamflow–base flow ratio in a lowland area of north-eastern Romania, Water Resour., 44, 579–585, https://doi.org/10.1134/S0097807817040121, 2017.

Minella, J. P. G., Merten, G. H., Schlesner, A., Bernardi, F., de Barros, C. A. P., Tiecher, T., Ramon, R., Evrard, O., dos Santos, D. R., Reichert, J. M., and Tassi, R.: Combining sediment source tracing techniques with traditional monitoring: The "Arvorezinha catchment" experience, Hydrol. Process., 36, e14665, https://doi.org/10.1002/hyp.14665, 2022.

Moriasi, D. N., Arnold, J. G., Van Liew, M. W., Bingner, R. L., Harmel, R. D., and Veith, T. L.: Model evaluation guidelines for systematic quantification of accuracy in watershed simulations, Trans. ASABE, 50, 885–900, https://doi.org/10.13031/2013.23153, 2007.

Moriasi, D. N., Gitau, M. W., Pai, N., and Daggupati, P.: Hydrologic and water quality models: Performance measures and evaluation criteria, Trans. ASABE, 58, 1763–1785, https://doi.org/10.13031/trans.58.10715, 2015.

Mugo, J. M. and Sharma, T. C.: Application of a conceptual method for separating runoff components in daily hydrographs in Kimakia forest catchments, Kenya, Hydrol. Process., 13, 2931–2939, https://doi.org/10.1002/(SICI)1099-1085(19991215)13:17<2931::AID-HYP838>3.0.CO;2-N, 1999.

https://doi.org/10.5194/egusphere-2025-244
Preprint. Discussion started: 26 March 2025

Munir, M. U., Blaurock, K., and Frei, S.: Understanding the vulnerability of surface-groundwater interactions to climate change: Insights from a Bavarian Forest headwater catchment, Environ. Earth Sci., 83, 11314, https://doi.org/10.1007/s12665-023-11314-2, 2024.

Murphy, R., Graszkiewicz, Z., Hill, P., Neal, B., and Nathan, R.: Australian rainfall and runoff. Project 7: Baseflow for catchment simulation. Stage 2 report, No. P7/S2/017, Engineers Australia, Canberra, Australia, 205 pp., 2011.

Murray, B. R., Zeppel, M. J. B., Hose, G. C., and Eamus, D.: Groundwater-dependent ecosystems in Australia: It's more than just water for rivers, Ecol. Manage. Restor., 4, 110–113, https://doi.org/10.1046/j.1442-8903.2003.00144.x, 2003.

Murray, J., Ayers, J., and Brookfield, A.: The impact of climate change on monthly baseflow trends across Canada, J. Hydrol., 618, 129254, https://doi.org/10.1016/j.jhydrol.2023.129254, 2023.

Mwakalila, S., Feyen, J., and Wyseure, G.: The influence of physical catchment properties on baseflow in semi-arid environments, J. Arid Environ., 52, 245–258, https://doi.org/10.1006/jare.2001.0947, 2002.

Narimani, R., Jun, C., Nezhad, S. M., Bateni, S. M., Lee, J., and Baik, J.: The role of climate conditions and groundwater on baseflow separation in Urmia Lake Basin, Iran, J. Hydrol. Reg. Stud., 47, 101383, https://doi.org/10.1016/j.ejrh.2023.101383, 2023.

Nash, J. E. and Sutcliffe, J. V.: River flow forecasting through conceptual models part I – A discussion of principles, J. Hydrol., 10, 282–290, https://doi.org/10.1016/0022-1694(70)90255-6, 1970.

Nathan, R. J. and McMahon, T. A.: Evaluation of automated techniques for baseflow and recession analyses, Water Resour. Res., 26, 1465–1473, https://doi.org/10.1029/WR026i007p01465, 1990.

Nathan, R. J. and Weinmann, P. E.: Low flow atlas for Victorian streams, Department of Conservation and Natural Resources, Melbourne, Australia, 43 pp., 1993.

Okello, A. M. L. S., Uhlenbrook, S., Jewitt, G. P. W., Masih, I., Riddell, E. S., and van der Zaag, P.: Hydrograph separation using tracers and digital filters to quantify runoff components in a semi-arid mesoscale catchment, Hydrol. Process., 32, 1334–1350, https://doi.org/10.1002/hyp.11491, 2018.

Partington, D., Brunner, P., Simmons, C. T., Therrien, R., Werner, A. D., Dandy, G. C., and Maier, H. R.: A hydraulic mixing-cell method to quantify the groundwater component of streamflow within spatially distributed fully integrated surface water–groundwater flow models, Environ. Model. Softw., 26, 886–898, https://doi.org/10.1016/j.envsoft.2011.02.007, 2011.

Pilgrim, D. H., Huff, D. D., and Steele, T. D.: Use of specific conductance and contact time relations for separating flow components in storm runoff, Water Resour. Res., 15, 329–339, https://doi.org/10.1029/WR015i002p00329, 1979.

Ramon, R.: Kinetic energy measurement of rainfall and defining a pluvial index to estimate erosivity in Arvorezinha, RS, MSc thesis, Centro de Ciências Rurais, UFSM, Santa Maria, Brazil, 87 pp., 2017.

Ramon, R., Minella, J. P. G., Merten, G. H., de Barros, C. A. P., and Canale, T.: Kinetic energy estimation by rainfall intensity and its usefulness in predicting hydrosedimentological variables in a small rural catchment in southern Brazil, Catena, 148, 176–184, https://doi.org/10.1016/j.catena.2016.07.015, 2017.

https://doi.org/10.5194/egusphere-2025-244
Preprint. Discussion started: 26 March 2025

Robson, A. and Neal, C.: Hydrograph separation using chemical techniques – an application to catchments in Mid-Wales, J. Hydrol., 116, 345–363, https://doi.org/10.1016/0022-1694(90)90132-H, 1990.

Rodhe, A. Chapter 12 - Snowmelt-Dominated Systems. In C. Kendall & J. J. McDonnell (Eds.), Isotope Tracers in Catchment Hydrology (pp. 391-433). Elsevier. https://doi.org/10.1016/B978-0-444-81546-0.50019-7, 1998.

Santarosa, L. V., Gastmans, D., Gilmore, T. E., Boll, J., Betancur, S. B., and Gonçalves, V. F. M.: Baseflow and water resilience variability in two water management units in southeastern Brazil, Int. J. River Basin Manage., 21, 387–400, https://doi.org/10.1080/15715124.2021.2002346, 2023.

Santos, H. G., Jacomine, P. K. T., Anjos, L. H. C., Oliveira, V. A., Lumbreras, J. F., Coelho, M. R., Almeida, J. A., Araujo Filho, J. C., Oliveira, J. B., and Cunha, T. J. F.: Brazilian soil classification system, 5th Edn., Brasília, DF, Brazil, Embrapa, available at: https://www.embrapa.br/busca-de-publicacoes/-/publicacao/1094001/brazilian-soil-classification-system (last access: January 2025), 2018.

Scanlon, T. M., Raffensperger, J. P., and Hornberger, G. M.: Modeling transport of dissolved silica in a forested headwater catchment: Implications for defining the hydrochemical response of observed flow pathways, Water Resour. Res., 37, 1071–1082, https://doi.org/10.1029/2000wr900278, 2001.

Serur, A. B.: Optimal surface water allocation under various scenarios in the Central Rift Valley basin in Ethiopia, Sustain. Water Resour. Manage., 8, https://doi.org/10.1007/s40899-022-00752-8, 2022.

Shao, G. W., Zhang, D. R., Guan, Y. Q., Sadat, M. A., and Huang, F.: Application of different separation methods to investigate the baseflow characteristics of a semi-arid sandy area, northwestern China, Water, 12, 20434, https://doi.org/10.3390/w12020434, 2020.

Silva, C. C., Minella, J. P. G., Schlesner, A., Merten, G. H., de Barros, C. A. P., Tassi, R., and Dambroz, A. P. B.: Unpaved road conservation planning at the catchment scale, Environ. Monit. Assess., 193, https://doi.org/10.1007/s10661-021-09398-z, 2021.

SKM and CSIRO: Methods for estimating groundwater discharge to streams – Summary of field trials, Summary report for the Australian Government, Water for the Future - Water Smart Australia Program, 67 pp., 2012.

Sloto, R. A. and Crouse, M. Y.: HYSEP: A computer program for streamflow hydrograph separation and analysis, U.S. Geological Survey Water-Resources Investigations Report 96-4040, 46 pp., https://doi.org/10.3133/wri964040, 1996.

Stewart, M. K.: Promising new baseflow separation and recession analysis methods applied to streamflow at Glendhu Catchment, New Zealand, Hydrol. Earth Syst. Sci., 19, 2587–2603, https://doi.org/10.5194/hess-19-2587-2015, 2015.

Stewart, M. K., Mehlhorn, J., and Elliott, S.: Hydrometric and natural tracer (oxygen-18, silica, tritium and sulphur hexafluoride) evidence for a dominant groundwater contribution to Pukemanga Stream, New Zealand, Hydrol. Process., 21, 3340–3356, https://doi.org/10.1002/hyp.6557, 2007.

Su, C. H., Costelloe, J. F., Peterson, T. J., and Western, A. W.: On the structural limitations of recursive digital filters for base flow estimation, Water Resour. Res., 52, 4745–4764, https://doi.org/10.1002/2015WR018067, 2016a.

https://doi.org/10.5194/egusphere-2025-244
Preprint. Discussion started: 26 March 2025

Su, C. H., Peterson, T. J., Costelloe, J. F., and Western, A. W.: A synthetic study to evaluate the utility of hydrological signatures for calibrating a base flow separation filter, Water Resour. Res., 52, 6526–6540, https://doi.org/10.1002/2015wr018177, 2016b.

Sun, Y. W., Xu, C. D., Ma, M. W., Liu, X. M., Liu, L., and Yu, F. R.: Annual, seasonal, and monthly baseflow trend in an arid area in Loss Plateau, China, Water Supply, 23, 4855–4875, https://doi.org/10.2166/ws.2023.322, 2023.

Tallaksen, L. M.: A review of baseflow recession analysis, J. Hydrol., 165, 349–370, https://doi.org/10.1016/0022-1694(95)92779-D, 1995.

Tan, S. B. K., Lo, E. Y.-M., Shuy, E. B., Chua, L. H., and Lim, W. H.: Hydrograph separation and development of empirical relationships using single-parameter digital filters, J. Hydrol. Eng., 14, 271–279, https://doi.org/10.1061/(ASCE)1084-0699(2009)14:3(271), 2009a.

Tan, S. B. K., Lo, E. Y. M., Shuy, E. B., Chua, L. H. C., and Lim, W. H.: Generation of total runoff hydrographs using a method derived from a digital filter algorithm, J. Hydrol. Eng., 14, 101–106, https://doi.org/10.1061/(ASCE)1084-0699(2009)14:1(101), 2009b.

Tan, X., Liu, B., and Tan, X.: Global changes in baseflow under the impacts of changing climate and vegetation, Water Resour. Res., 56, e2020WR027349, https://doi.org/10.1029/2020WR027349, 2020.

Tiecher, T., Caner, L., Minella, J. P. G., Evrard, O., Mondamert, L., Labanowski, J., and Rheinheimer, D. D.: Tracing sediment sources using mid-infrared spectroscopy in Arvorezinha catchment, southern Brazil, Land Degrad. Dev., 28, 1603–1614, https://doi.org/10.1002/ldr.2690, 2017.

Tiecher, T., Moura-Bueno, J. M., Caner, L., Minella, J. P. G., Evrard, O., Ramon, R., Naibo, G., de Barros, C. A. P., Silva, Y. J. A. B., Amorim, F. F., and Rheinheimer, D. S.: Improving the quantification of sediment source contributions using different mathematical models and spectral preprocessing techniques for individual or combined spectra of ultraviolet-visible, near- and middle-infrared spectroscopy, Geoderma, 384, 114815, https://doi.org/10.1016/j.geoderma.2020.114815, 2021.

Uzeika, T., Merten, G. H., Minella, J. P. G., and Moro, M.: Use of the SWAT model for hydro-sedimentologic simulation in a small rural watershed, Rev. Bras. Cienc. Solo, 36, 557–565, https://doi.org/10.1590/S0100-06832012000200025, 2012.

Vasconcelos, V. V., Martins Junior, P. P., and Hadad, R. M.: Estimation of flow components by recursive filters: Case study of Paracatu River Basin (SF-7), Brazil, Geol. USP Ser. Cient., 13, 3–24, https://doi.org/10.5327/Z1519-874X2013000100001, 2013.

Vogel, R. M. and Kroll, C. N.: Estimation of baseflow recession constants, Water Resour. Manage., 10, 303–320, https://doi.org/10.1007/BF00508898, 1996.

Vogel, R. M. and Kroll, C. N.: On the need for streamflow drought frequency guidelines in the US, Water Policy, 23, 216–231, https://doi.org/10.2166/wp.2021.244, 2021.

https://doi.org/10.5194/egusphere-2025-244
Preprint. Discussion started: 26 March 2025

Walker, G.: Risk of stream loss from changing irrigation, climate and groundwater extraction on the southern riverine plain of the Murray-Darling Basin in south-eastern Australia, Australas. J. Water Resour., 27, 289–310, https://doi.org/10.1080/13241583.2023.2181292, 2023.

Wels, C., Cornett, R. J., and Lazerte, B. D.: Hydrograph separation: A comparison of geochemical and isotopic tracers. J. Hydrol., 122,, 253-274, https://doi.org/10.1016/0022-1694(91)90181-G, 1991.

Wu, J., Miao, C., Duan, Q., Lei, X., Li, X., and Li, H.: Dynamics and attributions of baseflow in the semiarid Loess Plateau, J. Geophys. Res.-Atmos., 124, 3684–3701, https://doi.org/10.1029/2018JD029775, 2019.

Xie, J. X., Liu, X. M., Wang, K. W., Yang, T. T., Liang, K., and Liu, C. M.: Evaluation of typical methods for baseflow separation in the contiguous United States, J. Hydrol., 583, 124628, https://doi.org/10.1016/j.jhydrol.2020.124628, 2020.

Yang, W. F., Xiao, C. L., Zhang, Z. H., and Liang, X. J.: Can the two-parameter recursive digital filter baseflow separation method really be calibrated by the conductivity mass balance method? Hydrol. Earth Syst. Scii, 25, 1747-1760. https://doi.org/10.5194/hess-25-1747-2021, 2021.

Yao, L., Sankarasubramanian, A., and Wang, D.: Climatic and landscape controls on long-term baseflow, Water Resour. Res., 57, e2020WR029284, https://doi.org/10.1029/2020WR029284, 2021.

Zhang, J. L., Zhang, Y. Q., Song, J. X., and Cheng, L.: Evaluating relative merits of four baseflow separation methods in Eastern Australia, J. Hydrol., 549, 252–263, https://doi.org/10.1016/j.jhydrol.2017.04.004, 2017.

Zhang, R. G., Li, Q., Chow, T. L., Li, S., and Danielescu, S.: Baseflow separation in a small watershed in New Brunswick, Canada, using a recursive digital filter calibrated with the conductivity mass balance method, Hydrol. Process., 27, 2659–2665, https://doi.org/10.1002/hyp.9417, 2013.